OCA-B promotes autoimmune demyelination through control of stem-like CD4+ T cells

Erik P. Hughes[1,3], Amber Syage[1,3], Elnaz Mirzaei Mehrabad[2,3,5], Thomas E. Lane[5], Benjamin T. Spike[2,3], Dean Tantin[1,3]

[1]Department of Pathology, University of Utah School of Medicine, Salt Lake City, UT 84112 U.S.A.
[2]Department of Oncological Sciences, University of Utah School of Medicine, Salt Lake City, UT 84112 U.S.A.
[3]Huntsman Cancer Institute, University of Utah School of Medicine, Salt Lake City, UT 84112 U.S.A.
[4]Univeristy of Utah School of Computing, Salt Lake City, UT, 84112 U.S.A
[5]Department of Neurobiology and Behavior, School of Biological Sciences, University of California, Irvine, CA 92697, U.S.A.
e-mail dean.tantin@path.utah.edu

Short title: OCA-B promotes CD4+ T cell mediated demyelinating disease

Keywords OCA-B/Bob1/Pou2af1; autoimmunity; multiple sclerosis; EAE; stem-like CD4+ T cells; relapsing-remitting

Words in abstract: 150
Words main text: 4,396
Total main display items: 6

Summary

Stem-like T cell populations can selectively promote autoimmunity, but the activities that sustain these populations are incompletely understood. Here, we show that T cell-intrinsic loss of the transcription cofactor OCA-B protects mice from experimental autoimmune encephalomyelitis (EAE) while preserving responses to infection. In EAE models driven by antigen re-encounter, OCA-B deletion eliminates CNS infiltration, proinflammatory cytokine production and clinical disease. OCA-B-expressing $CD4^+$ T cells within the CNS of mice with EAE display a memory phenotype and preferentially confer disease. In a relapsing-remitting EAE model, OCA-B T cell-deficiency specifically protects mice from relapse. During remission, OCA-B promotes the expression of *Tcf7*, *Slamf6*, and *Sell* in proliferating T cell populations. At relapse, OCA-B loss results in both the accumulation of an immunomodulatory $CD4^+$ T cell population expressing *Ccr9* and *Bach2*, and the loss of effector gene expression from Th17 cells. These results identify OCA-B as a driver of pathogenic stem-like T cells.

Introduction

2.5 million individuals worldwide suffer from multiple sclerosis (MS), with almost 1 million cases in the United States[1]. Despite recent advances, the development of new therapies that block MS while sparing immunosurveillance mechanisms needed to prevent infection and viral recrudescence remains a critical goal. Genome-wide association studies (GWAS) identify the *HLA* loci as the most important determinant of MS pathogenesis, emphasizing the impact of T cells in MS[2,3]. The association with the major histocompatibility complex (MHC) class II locus in particular indicates that myelin-specific $CD4^+$ T cells are key regulators of disease.

The predominant preclinical model of MS is experimental autoimmune encephalomyelitis (EAE), in which laboratory animals are immunized with myelin-specific proteins or peptides to activate antigen specific $CD4^+$ T cells that infiltrate the central nervous system (CNS) and mediate disease. EAE within the C57BL/6 mouse background establishes chronic disease. In these models, Th1 and Th17 effector $CD4^+$ T cell subsets are pathogenetic mediators[4,5]. After accessing the CNS, these cells promote neuroinflammation through the secretion of interferon-gamma (IFNγ), interleukin-17 (IL-17), granulocyte macrophage stimulating-factor (GM-CSF) and other inflammatory mediators and chemoattractants that recruit the cell types responsible for driving demyelination[6–8].

Myelin-reactive T cells from the blood of MS patients show stem/memory-like properties, with reduced need for co-stimulation, suggesting signs of previous activation[9–12]. Consistent with these findings, autoreactive and bystander memory-phenotype $CD4^+$ T cells preferentially transfer demyelinating disease in mouse models[13–15]. While these studies have identified vital $CD4^+$ T cell populations in EAE, further research on the mechanisms creating and sustaining these populations is required to develop more precise therapies.

Oct1, a POU domain transcription factor encoded by *Pou2f1*, has been linked to autoimmune states. GWAS studies have identified Oct1 binding site polymorphisms that associate with a predisposition for autoimmune diseases, including MS[16–19]. In $CD4^+$ T cells, Oct1 promotes interchromosomal interactions important for T cell polarization and effector function[20–23]. Additionally, Oct1 promotes the development of both $CD4^+$ memory[23] and EAE pathogenesis and demyelination. In contrast, Oct1 loss preserves immune responses to the neurotrophic viral infection[20]. These observations highlight a promising therapeutic window in which targeting this pathway may limit autoimmune CNS demyelination without the broad immune suppression elicited by many current therapeutics. However, Oct1 is widely expressed and regulates both embryonic development and somatic stem cell function[24–26], making it a poor therapeutic target.

77 The lymphoid-restricted transcription cofactor OCA-B regulates transcription by docking
78 with Oct1, and in B cells an additional related factor, Oct2[27]. In contrast to Oct1, OCA-B whole-
79 body knockouts are viable and fertile[28]. Polymorphisms in the *Ocab* (*Pou2af1*) locus are
80 associated with autoimmune diseases, including MS[29,30]. Targeting either OCA-B by genetic
81 deletion in T cells or its downstream pathways with a peptide mimic suppresses type-1 diabetes[31].
82 OCA-B interacts with target genes such as *Il2, Ifng, Il21, Csf2 (Gmcsf), Tnfrsf4 (Ox40), Icos* and
83 *Ctla4*, but is dispensable for their expression following primary activation of T cells. Instead, OCA-
84 B regulates these targets under a narrow range of conditions, for example following secondary
85 stimulation in culture[23]. Many of these targets are directly implicated in MS pathogenesis[6–8,32–38].
86 OCA-B controls expression of the *Tbx21* (*Tbet*), which encodes a key regulator of Th1 effector
87 responses, but also promotes Th17 differentiation and interacts with RORγt, a key regulator of
88 Th17 cells[23,39,40]. In the context of MS, the only published work used OCA-B whole body knockouts
89 and showed measurable but incomplete protection in chronic C57BL/6 EAE models[40].
90 Cumulatively, these findings indicate that OCA-B plays poorly defined but possibly significant
91 roles in MS pathogenesis.
92 Here, we show that OCA-B within the T cell compartment drives EAE by promoting
93 pathogenic maturation of stem-like $CD4^+$ T cells. In C57BL/6 mice, T cell OCA-B loss significantly
94 protects mice from chronic EAE, while preserving responses to the neurotrophic coronavirus
95 JHMV. Using Th1 and Th17 adoptive transfer assays, we show that OCA-B is essential for the
96 infiltration of pathogenic CNS-infiltrating cells and clinical disease. Using an OCA-B reporter
97 mouse, we find that OCA-B expressing $CD4^+$ T cells taken from MOG peptide primed mice are
98 stem-like and preferentially transfer demyelinating disease, highlighting OCA-B as a marker and
99 promoter of encephalitogenic autoimmune $CD4^+$ T cell activity. Intriguingly, T cell conditional
100 OCA-B knockout In EAE models on the autoimmune-prone non-obese diabetic (NOD)
101 background, which develops a relapsing-remitting disease[41], specifically protects against relapse.
102 Single cell transcriptomic analysis of $CD3\varepsilon^+$ CNS-infiltrating T cells at remission and relapse
103 indicates that OCA-B promotes disease relapse through control of stem-like T cell populations,
104 driving them to pathogenic Th17 differentiation.

105 **Results**

106 **OCA-B promotes chronic EAE in C57BL/6 mice**

107 To understand the impact of OCA-B in T cell mediated autoimmunity, we utilized an *Ocab*
108 (*Pou2af1*) conditional knockout allele crossed to the CD4-Cre driver which efficiently deletes
109 OCA-B in T cells[31]. We induced EAE in C57BL/6 female *Ocab*$^{fl/fl}$;CD4-Cre mice and littermate
110 *Ocab*$^{fl/fl}$ controls through subcutaneous (s.c.) injection of myelin oligodendrocyte glycoprotein
111 $(MOG)_{35-55}$ peptide in Complete Freund's Adjuvant (CFA) followed by intraperitoneal (i.p.)
112 injections of *Bordetella pertussis* toxin. *Ocab*$^{fl/fl}$;CD4-Cre mice showed reduced chronic EAE
113 clinical scores and weight loss (Fig. 1a, b). Spinal cords were taken at peak disease (day 15) for
114 histological analysis. Luxol fast blue (LFB) staining in combination with hematoxylin and eosin
115 (H&E) was used to evaluate differences in demyelination between groups. *Ocab*$^{fl/fl}$;CD4-Cre mice
116 showed a significant decrease in spinal cord demyelination compared to littermate *Ocab*$^{fl/fl}$
117 controls (Fig. 1c, d). Peak disease flow cytometric profiling showed decreased $CD4^+$ T cell
118 infiltration into the CNS of *Ocab*$^{fl/fl}$;CD4-Cre mice, however no differences in other infiltrating cell
119 populations or in the relative proportions of the proinflammatory cytokines IFNy, IL-17, or GM-
120 CSF were observed (Fig. 1e, f, and Extended Data Fig. 1a-c). As no differences in the frequency
121 of cytokine expression were observed across total T cell populations, we studied MOG-specific
122 $CD4^+$ T cells using the MHC class II I-A^b MOG_{38-49} tetramers. At peak disease, *Ocab*$^{fl/fl}$;CD4-Cre
123 mice showed a trending reduction in MOG tetramer-specific cell frequency (p=0.055) and a
124 significant reduction in numbers (p=0.003) compared to controls (Fig. 1g, h). These results
125 indicate that the protection conferred by OCA-B loss in T cells is marked by modest decreases in
126 MOG-specific $CD4^+$ T cells within the CNS, resulting in fewer pathogenic T cells driving
127 demyelination.

128

129 **OCA-B is essential for EAE mediated by adoptive transfer of Th1- and Th17-polarized T**
130 **cells**

131 MS is driven by autoreactive $CD4^+$ Th1 and Th17 cells within the CNS that recruit $CD8^+$ T cells,
132 macrophages, microglia and neutrophils, which together mediate white-matter damage[42]. To
133 investigate the impact of OCA-B on autoimmune Th1 and Th17 populations, we used adoptive
134 transfer EAE models with female *Ocab*$^{fl/fl}$;CD4-Cre and *Ocab*$^{fl/fl}$ littermate controls. Mice were
135 primed with MOG_{35-55} in CFA for 10-14 days (MOG-primed). $CD4^+$ T cells were purified from the
136 lymph nodes of primed mice and polarized in vitro into Th1 and Th17 cells as previously
137 described[43,44]. 3×10^6 Th1- or Th17-polarized $CD4^+$ cells from experimental or control donors were

138 transferred into wild-type male C57BL/6 recipients by i.p. injection. EAE onset in mice receiving
139 either Th1- or Th17-polarized control cells was rapid and severe (Fig. 2a, b). In contrast to the
140 mild protection observed with OCA-B deficiency in standard C57BL/6 EAE, mice adoptively
141 transferred with T cells lacking OCA-B were strongly protected from clinical disease regardless of
142 their polarization state. Interestingly, the ability to initially polarize $CD4^+$ T cells into Th1 and Th17
143 effectors in vitro was minimally affected by OCA-B loss (Extended Data Fig. 2), whereas the same
144 engrafted T cells taken from the CNS of Th17 recipient mice at day 15 not only showed decreased
145 CNS infiltration but also poor IL-17 expression (Fig. 2c-e). These results indicate a central role for
146 OCA-B in promoting robust inflammatory T cell responses upon antigen reencounter in adoptive
147 transfer EAE models.

148 To test the hypothesis that OCA-B within T cells promotes robust cytokine responses of
149 Th17 cells upon secondary encounter, we combined an in vitro T cell restimulation response
150 assay[45,46] with Th17 differentiation. Naïve splenic $CD4^+$ T cells isolated from male C57BL/6
151 *Ocab*$^{fl/fl}$;CD4-Cre or *Ocab*$^{fl/fl}$ control mice were stimulated for 2 days with anti-CD3ε/CD28
152 antibodies during a 5 day Th17 polarization using recombinant IL-23, IL-1α and anti-IFNγ. The
153 cells were rested for 8 days after primary stimulation, then restimulated with anti-CD3ε/CD28 (Fig.
154 2f). Minimal differences in proinflammatory cytokine expression between groups were observed
155 after initial stimulation and differentiation, however OCA-B deficient $CD4^+$ T cells showed a
156 marked reduction in IFNγ and IL-17 production upon restimulation (Fig. 2g, h). This result shows
157 that OCA-B is selectively required for robust Th17 responses upon secondary antigen encounter
158 in vitro.
159

160 **OCA-B is dispensable for neurotropic viral clearance**

161 To investigate if T cell OCA-B deletion impacts the ability to mount immune responses and control
162 viral infection in the CNS, male *Ocab*$^{fl/fl}$;CD4-Cre and *Ocab*$^{fl/fl}$ littermate controls were inoculated
163 with 1500 plaque-forming units (PFU) of the John H. Muller strain of murine hepatitis (JHMV), a
164 β-coronavirus adapted to infect glial cells (astrocytes, microglia and oligodendrocytes) in the
165 mouse brain and spinal cord. Intracranial inoculation with JHMV results in acute
166 encephalomyelitis and chronic demyelination that is similar to autoantigen-driven EAE. Disease
167 severity was determined by evaluating JHMV clinical scores over 21 days post-infection (dpi).
168 *Ocab*$^{fl/fl}$;CD4-Cre animals showed negligible differences in clinical scores compared to *Ocab*$^{fl/fl}$
169 littermates (Fig. 3a), suggesting that OCA-B loss does not limit baseline T cell responses to acute

170 infection. Spinal cords were taken on 21 dpi for histological analysis to investigate differences in
171 demyelination. LFB histology of brain tissue at 21 dpi showed no significant differences in
172 demyelination between OCA-B deficient and control infected animals (Fig. 3b, c). Flow cytometric
173 analysis of brain tissue showed no significant differences in infiltrating $CD4^+$ T cell numbers at dpi
174 7, 12, and 21 (Fig. 3d), however at later timepoints (21 dpi), OCA-B deficient mice did show a
175 slightly decreased frequency of IFNγ producing $CD4^+$ T cells but no difference in total numbers
176 (Fig. 3e, f, and Extended Data Fig. 3a). Interestingly, there were also more IFNγ-producing $CD8^+$
177 T cells in OCA-B deficient animals at 12 dpi (Extended Data Fig. 3b-d). Viral titers of brain
178 homogenate were collected on 7, 12 and 21 dpi to measure viral clearance. *Ocab*$^{fl/fl}$;CD4-Cre and
179 *Ocab*$^{fl/fl}$ littermate control animals showed similar titers at dpi 7 and 12, and virus was undetectable
180 at day 21 regardless of genotype (Fig. 3g). This result suggests that OCA-B is dispensable for
181 immune responses to and clearance of neurotropic viruses.
182
183 **OCA-B expressing $CD4^+$ T cells display pathogenic stem-like properties and preferentially**
184 **transfer demyelinating disease**
185 We used a recently described an OCA-B reporter (OCA-B-mCherry) mouse which selectively
186 labels OCA-B expressing B and T cells with mCherry[47] to evaluate OCA-B expression within CNS
187 infiltrating T cells. Female C57BL/6 homozygous OCA-B-mCherry reporter mice were induced
188 with MOG_{35-55} EAE and assessed by flow cytometry at peak clinical disease. Flow cytometric
189 analysis of CNS-infiltrating mCherry-positive $CD4^+$ T cells showed increased CD44 and CD62L
190 co-expression, indicative of memory-like properties in the OCA-B expressing T cell population
191 (Fig. 4a). The association of OCA-B expression with memory-like profile was observed in the
192 brain, spine and draining cervical lymph nodes (Fig. 4b).
193 Memory-like $CD4^+$ T cells have been implicated as major orchestrators of autoimmune
194 demyelination in mice and humans[9–12,14,15,48]. To see if this memory-like profile of OCA-B
195 expressing $CD4^+$ T cells is specific to CNS infiltrating cells, we performed flow cytometry using
196 draining lymph node and splenic T cells from MOG-primed OCA-B-mCherry reporter mice. Similar
197 to OCA-B^+ CNS infiltrating cells, OCA-B expressing $CD4^+$ T cells within the cervical lymph node
198 and spleen showed increased CD44 and CD62L co-expression (Fig. 4c, d).
199 We next evaluated OCA-B-mCherry positive and negative populations by RNA
200 sequencing of $CD4^+$ T cells isolated from the lymph nodes of 14-day MOG-primed mice. ~1500
201 genes were upregulated and ~350 downregulated in the OCA-B expressing compared to OCA-B

202 negative cells (Supplementary Table 1). Upregulated genes within OCA-B expressing cells
203 include *Cxcr6*, *Slamf6*, *Il23r*, *Rorc*, *Ifng*, and *Il17a* while downregulated genes include *Foxp3*, *Il7r*
204 and *Ccr9* (Fig. 4e, f). Expression of *Tcf7* (which encodes TCF-1) was high within both OCA-B
205 positive and negative populations (Supplementary Table 1). Gene ontology (GO) and pathway
206 analysis of upregulated genes show enrichment for autoimmune diseases including lupus,
207 autoimmune thyroid disease, and type 1 diabetes (*Il2*, *Cd28*, *Ifng*) (Fig. 4g, and Supplementary
208 Table 2).

209 To determine if OCA-B expression marks highly pathogenic $CD4^+$ T cell populations, we
210 used the OCA-B-mCherry reporter mice as donors in adoptive transfer EAE. 11-week-old male
211 and female littermates homozygous for the OCA-B-mCherry reporter were primed for 14 days
212 with MOG_{35-55} in CFA as previously described[44]. $CD4^+$ T cells were isolated from spleen and lymph
213 nodes and sorted based on mCherry expression (Extended Data Fig. 4a). 9×10^5 mCherry
214 negative and positive cells were cultured in Th1 polarizing conditions and subsequently
215 transferred into C57BL/6 recipients as previously described[14]. Adoptive transfer disease
216 progression was measured by clinical score and normalized weight. Recipients of OCA-B-
217 expressing mCherry positive cells showed increased clinical disease severity and weight loss
218 compared to mCherry negative recipients (Fig. 4h, and Extended Data Fig. 4b). These findings
219 indicate that OCA-B marks $CD4^+$ T cells with pathogenic stem-like gene expression and can be
220 used to prospectively identify peripheral $CD4^+$ T cells with encephalitogenic properties.
221

222 **OCA-B promotes neuroinflammation in relapsing-remitting EAE models via control of**
223 **stem/memory-like T cell populations**

224 In contrast to the chronic form of EAE that develops in C57BL/6 mouse models, EAE on the NOD
225 background exhibits a relapsing-remitting pattern that more closely mimics human disease[41]. To
226 study the impact of OCA-B loss in T cells on mouse models that more closely resemble human
227 MS disease patterns, we utilized a previously generated *Ocab* T cell conditional knockout allele
228 crossed to the NOD mouse background[31]. EAE was induced in 15-18 week old female
229 NOD.*Ocab*$^{fl/fl}$;CD4-Cre and littermate control NOD.*Ocab*$^{fl/fl}$ mice with MOG_{35-55}. Clinical scores and
230 weights were recorded for 47 days to observe initial disease onset, relapse and relapse recovery.
231 No significant differences in clinical scores were observed between groups at disease onset (day
232 10-19), however following the primary remission, NOD.*Ocab*$^{fl/fl}$;CD4-Cre animals were almost
233 completely protected against disease relapse (Fig. 5a). Individual NOD mouse clinical scores are

shown in Extended Data Fig. 5a-b. Normalized weights of animals also reflected the protective effect of OCA-B loss in T cells at the relapse timepoint (Fig. 5b).

To understand differences in CNS-infiltrating T cells underlying relapse protection at a population and transcriptional level, we performed single-cell RNA sequencing (scRNAseq) of CD3ε$^+$ T cell isolates from CNS (brain + spinal cord) at remission (day 24) and peak relapse (day 33). Cells from 3-6 NOD.*Ocab*$^{fl/fl}$;CD4-Cre and NOD.*Ocab*$^{fl/fl}$ littermate controls were collected and combined for analysis. 7799 (remission) to 9224 (relapse) *Ocab* knockout and 6009 (remission) to 7525 (relapse) control cells were used for analysis, with an average read per cell ranging from 90,000 to 190,000. For remission, Uniform Manifold Approximation and Projection (UMAP) clustering using both genotypes revealed 16 clusters corresponding to a broad T cell repertoire consisting of natural-killer T (NKT) cells (the largest cluster) and different CD4$^+$ and CD8$^+$ subsets (Fig. 5c). Noteworthy clusters based on mRNA expression included proliferating (*Ki67*, *Pcna*, *Mcm2*), Th1-like (*Tbx21*, *Ifng*, *Tnf*, *Il12rb2*) and Treg (*Foxp3*, *Ctla4*) (Supplementary Table 3). Feature plots for *Foxp3* and *Mki67* are shown in Fig. 5d. Additional feature plots for *Cxcr6*, *Il23r* and *Bach2* are shown in Extended Data Fig. 5c. Notably there was a large decrease in NKT cell numbers in knockout mice (36% control vs. 14% experimental). Within this cluster, changes in gene expression between control and conditional knockout groups were minimal. Most NKT cells from both groups showed a limited inflammatory cytokine response, consistent with the lack of clinical disease at remission (Extended Data Fig. 5d). The decrease in the large NKT population in the experimental group proportionally increases the percentage contribution of the other cells, and therefore similar or decreased percentages of these smaller clusters may identify populations of cells which promote relapse. Differential gene expression analysis of key clusters (Treg, Proliferating, and Th1-like) revealed increased expression of *Slamf6* in Tregs from experimental animals, while control animals showed increased markers associated with quiescence (*Btg1* and *Samhd1*), memory/stemness (*Slamf6*, *Tcf7*, and *Sell*) and pathogenicity (*Tcf7* and *Tox* co-expression) in proliferating and Th1-like cells (Fig. 5e). Spectral cytometry showed no significant difference in the frequency of CNS infiltrating CD4$^+$ T cells between groups at remission (Fig. 5f). However, OCA-B deficient CD4$^+$ T cells did show a significant reduction in CXCR6 and IFNγ/GM-CSF co-expression, indicative of reduced Th17 pathogenicity (Fig. 5g-i). These results indicate that loss of OCA-B in T cells selectively reduces proliferation and differentiation of pathogenic stem/memory-like CD4$^+$ T cells during disease remission.

NKT cell populations were normalized at relapse, and multiple stem-like and effector CD4$^+$ and CD8$^+$ T cell populations were present (Fig. 6aand Extended Data Fig. 6a; Supplementary

267 Table 4). TCR sequencing revealed an expansion of a subset of TCR clones in the OCA-B
268 deficient CD8 clusters while that most other clusters were highly polyclonal (Fig. 6b). Comparing
269 the 10 most expanded TCR clonotypes between knockouts and controls, there were several
270 shared clonotypes that were differentially expanded (Extended Data Fig. 6b and Supplementary
271 Table 5). A "Ccr9 stem-like" cluster expressing the gut homing chemokine receptor *Ccr9*, as well
272 as *Ccr7*, *Bach2*, and *Tcf7* was notably present (Fig. 6c). TCR clonotype analysis indicated that
273 this population was highly polyclonal (Fig. 6b). Additionally, a "Stem-like CD4-2" cluster
274 expressing *Tcf7*, Ccr7, *Bach2, Cd44* and low-level Cxcr6, and a prominent "Th17-like" cluster
275 expressing *Tcf7, Cd44*, *Il1r1, Lgals3*, and higher levels of *Cxcr6* was identified (Fig. 6c). This latter
276 cluster likely contains pathogenic effector cells. In the absence of OCA-B, several clusters showed
277 major changes in the percentage of cells including most prominently the Ccr9-stem-like cells (Fig.
278 6d). Feature plots comparing OCA-B T cell deficient mice to littermate controls for *Ccr9* and the
279 transcription factors *Tcf7* and *Bach2* are shown in Fig. 6d. The cells were also marked by the
280 expression of *Cd4*, *Tox, Ccr7, Ccr4* and limited expression of *Sell* (Extended Data Fig. 6c).
281 RNA velocity analysis of spliced and unspliced transcripts[49] identified clusters of T cells,
282 most bearing static gene expression profiles consistent with terminal differentiation, but some with
283 differentiating or transitional gene expression (Fig. 6e). Notably, OCA-B knockout cells showed
284 increased transcriptional stasis within the Ccr9-stem-like and proliferating clusters, and a
285 decreased transcriptional directionality of Th17 cells towards gd17 cells, the latter of which
286 express high levels of pathogenic markers including *Il1r1*, *Cxcr6*, and *Lgals3* (Extended Data Fig.
287 6a). Pseudotime analysis identified a transcriptional capacity in the control *Ccr9* expressing
288 population to differentiate into pathogenic Th17-like cells, whereas cells lacking OCA-B were
289 limited in this capacity, possibly resulting in the accumulation of these cells (Extended Data Fig.
290 6d). These changes culminated in the Th17-like effector knockout cells expressing reduced
291 pathogenicity-associated genes such as *Pdcd1*, *Tigit* and *Il1r1* (Fig. 6f). Together these results
292 suggest OCA-B mediates the transition of non-pathogenic stem-like cells to pathogenic Th17 cells
293 which ultimately drive disease relapse.

294 **Discussion**

295 The development of therapies that inhibit autoimmunity while minimizing impacts on normal
296 immune function remains a critical unmet goal in the field. In this study, we show that expression
297 of the transcriptional co-regulator OCA-B promotes a pathogenic, stem/memory-like function in T
298 cells, resulting in the establishment of CNS autoimmunity, and in particular episodes of relapse.
299 Loss of OCA-B attenuates these populations in chronic EAE, in adoptive transfer EAE, and in
300 NOD.EAE during episodes of remission. During relapse, OCA-B T cell knockout mice are almost
301 completely protected, and accumulate an immunomodulatory population of $CD4^+$ T cells
302 expressing *Ccr9*, *Bach2*, and *Tcf7*. OCA-B expression also marks viable pathogenic
303 stem/memory-like $CD4^+$ T cells that preferentially transfer EAE. Furthermore, the effects of
304 modulating OCA-B are EAE-selective, as responses to infection with a neurotropic coronavirus
305 were largely unaffected.

306 OCA-B docks with Oct1 upon $CD4^+$ T cell activation to poise immunomodulatory genes
307 such as *Il2*, *Ifng*, *Il17a*, Tbx21 (T-bet) and *Csf2* (*Gmcsf*) for robust expression upon antigen
308 reencounter[23,31]. Notably, unlike transcription factors such as NF-AT, AP-1 and NF-κB, Oct1 and
309 OCA-B are dispensable for normal primary T cell responses[23]. This finding predicts important
310 roles for OCA-B in $CD4^+$ T cells specifically in situations of antigen reencounter, which is a
311 necessary feature of autoimmunity. Conditional knockout of Oct1 in $CD4^+$ T cells reduces EAE
312 severity, with reduced proinflammatory cytokine expression and increased anergy[20]. Deletion of
313 Oct1 in T cells was dispensable for neurotropic viral clearance[20], however the ubiquitous
314 expression of Oct1 in adult tissue limits its translational potential. In contrast, the Oct1 coregulator
315 OCA-B is expressed primarily in B and T cells, and whole-body knockout mice are viable and
316 fertile[50], suggesting a druggable target. OCA-B is highly expressed in B cells and required for
317 germinal center formation[51,52]. OCA-B is expressed in $CD4^+$ T cells upon activation but maintained
318 at levels 50-100-fold less than in B cells[31,53,54]. This suggests that with proper therapeutic dosing,
319 OCA-B could be inhibited selectively in T cells with minimal impact to the B cell compartment.
320 Consistently, short-term administration of an OCA-B peptide mimic that inhibits OCA-B's
321 downstream effector functions reverses spontaneous type-1 diabetes in NOD mice[31]. However,
322 the toxicity limits its efficacy, including within EAE models. Further research is required for the
323 development of safe and effective OCA-B inhibitors.

324 OCA-B whole body knockout animals are protected from EAE, however, due to the
325 important role of OCA-B in humoral immunity it remained unclear if the protection observed is T
326 cell-derived[40]. Here we show that OCA-B promotes EAE pathogenesis through T cells.

327 Opportunistic infections and reactivation of latent CNS-tropic viruses are significant barriers for
328 MS therapeutics that focus on global immune suppression as a therapeutic mechanism. When
329 OCA-B T cell conditional knockout mice are challenged with the neurotropic coronavirus JHMV,
330 there is little difference in their ability to mount immune responses and control virus replication.
331 This finding indicates that OCA-B operates through a more precise mechanism that provides a
332 potential therapeutic window in which targeting OCA-B could be used to blunt autoimmunity while
333 sparing baseline immune responses.

334 Unlike the significant but modest protection observed in chronic C57BL/6 EAE, OCA-B
335 loss in adoptive transfer EAE almost completely protects recipient animals from disease. This
336 may indicate that adoptive transfer EAE models are more akin to autoantigen rechallenge where
337 transferred T cells become quiescent within the recipient before accessing the CNS and
338 promoting disease. Protection was observed regardless of whether donor cells were Th1- or
339 Th17-polarized, indicating that OCA-B functions through a mechanism that operates in parallel to
340 T cell polarization. Because OCA-B appears to operate in parallel to the Th1/Th17 paradigm, we
341 sought other mechanisms that might explain why knockout of this factor produces the strong
342 protection.

343 Recent findings indicate an emerging role for stem/memory-like T cells in promoting
344 autoimmunity[48,55]. For example, myelin-specific $CD4^+$ T cells in MS patients show signs of a
345 previously activated, memory-like phenotype when compared to healthy controls[9,10,12].
346 Furthermore, memory-like Th1 and Th17 cells are increased in the peripheral blood of MS patients
347 and display increased pathogenicity when compared to conventional Th17 Cells[56]. Similarly, in
348 EAE models, peripheral central memory-like $CD4^+CD44^{hi}CD62L^{hi}$ T cells confer increased
349 disease severity upon transfer[14]. Oct1 and OCA-B both promote the generation and functionality
350 of long-lived $CD4^+$ memory T cells[23,47]. We recently reported the generation of an OCA-B-mCherry
351 reporter mouse which effectively labels memory progenitor $CD4^+$ T cells during acute infection[47].
352 Similarly, OCA-B^{hi} $CD4^+$ T cells preferentially confer EAE, and reporter cells taken from the CNS
353 at peak EAE selectively express stem/memory markers. Further profiling OCA-B^{hi} $CD4^+$ T cells
354 suggests OCA-B promotes the transition of non-pathogenic stem-like cells to a pathogenic state
355 associated with markers such as *Cxcr6*, *Slamf6*, *Ifng*, and *Il17a*. The connection between OCA-
356 B expression and memory/stem-like T cells likely has not been observed before because OCA-B
357 is expressed at levels too low to be reproducibly captured with current single-cell RNA-seq
358 technologies.

359 Relapsing-remitting EAE models have been developed using the Swiss Jim Lambert (SJL)
360 and autoimmune prone non-obese diabetic (NOD) backgrounds[41,57]. In NOD mice, MOG_{35-55} EAE
361 has been described as relapsing-remitting with minimal initial disease that increases in severity
362 upon relapse[58,59]. Using this model with the conditional allele backcrossed to the NOD
363 background[31], we found that OCA-B T cell loss leaves initial clinical presentation minimally
364 affected but instead protects animals specifically at relapse. The finding that OCA-B loss in
365 conventional C57BL/6 EAE results in partial protection intermediate between the initial and
366 relapse phases of NOD.EAE suggests that chronic C57BL/6 EAE may not model either initial
367 presentation or relapse accurately, and instead represents a superposition of the two.
368 Single-cell RNA expression profiling at remission identifies a significant loss of *Slamf6*,
369 *Tcf7* (TCF1), and *Sell* from proliferative stem-like $CD4^+$ T cells in the OCA-B deficient condition.
370 While the majority of research on TCF-1-expressing stem-like T cells focuses on $CD8^+$
371 populations with the capacity for self-renewal and differentiation into effector cells, analogous
372 descriptions have been made for $CD4^+$ populations[48,60,61]. Indeed, autoimmune $CD4^+$ T cells
373 expressing these memory/stem-like markers have been reported as an encephalitogenic
374 reservoir that play a key role in EAE pathogenicity[48]. In the same study, bulk RNA sequencing
375 associated OCA-B expression within this stem-like reservoir[48].
376 Relapse timepoints were marked the by emergence of multiple populations of effector T
377 cells, and by the accumulation of a unique population of $CD4^+$ cells in OCA-B T cell deficient mice.
378 These cells are conspicuously marked by expression not only of *Ccr4*, but also of *Ccr9*, which
379 encodes a gut-homing chemokine receptor. $CCR9^+$ memory-like $CD4^+$ T cells have been linked
380 to MS and EAE protection[62]. The cells also express *Bach2*, a transcription regulator which was
381 recently associated with non-pathogenic immunomodulatory Th17-polarized cells in the context
382 of C57BL/6 EAE[63]. Although the *Bach2* change was concentrated in a specific cluster, in bulk
383 RNA-seq *Bach2* mRNA was still significantly downregulated ($p<10^{-13}$), although with a -1.74 fold
384 change (Supplementary Table 1). In B cells, OCA-B is known to regulate *Bach2*[64]. Velocity and
385 pseudotime analysis indicates that these cells are normally transcriptionally inclined to progress
386 towards an highly pathogenic Th17 population, but that progression stalls in mice whose T cells
387 lack OCA-B. Consistently, the Th17 effector population in these mice completely lack expression
388 of key genes such as *Il1r1* and *Pdcd1*, both of which are associated with pathogenicity in CNS-
389 infiltrating Th17 cells[48,64]. The cumulative alterations in these populations in OCA-B knockouts
390 likely explains why these mice are strongly protected against disease relapse. In conclusion, our

391 study indicates a prominent role for OCA-B in driving stem-like $CD4^+$ T cell populations towards
392 a pathogenic state while playing a minimal role in acute antiviral responses to a CNS infection.

393 **Figure legends**

394 **Fig.1 I OCA-B loss protects animals from chronic EAE**

395 **a,** *Ocab*$^{fl/fl}$ (n=16) and *Ocab*$^{fl/fl}$;CD4-Cre (n=22) mice were injected with MOG_{35-55} peptide in CFA
396 and *pertussis* toxin to induce EAE. Clinical scores were evaluated after EAE induction to
397 determine disease progression. **b,** Animal weights were recorded to evaluate weight loss as a
398 measurement of disease progression. **c,** Representative H&E/LFB staining of thoracic sections
399 taken from mice 15 days after EAE induction. Areas of demyelination are marked by black outline.
400 **d,** Quantification of demyelination in n=5 experimental and control mice. **e,** Brain and spinal cords
401 were isolated on day 15 of EAE and analyzed by spectral cytometry. Representative flow
402 cytometry plots of $CD45^+TCR\beta^+$ CNS infiltrating T cells showing frequency of $CD4^+$ and $CD8^+$ T
403 cells. **f,** Quantification of CNS infiltrating $CD4^+$ T cells. **g,** Representative plots showing frequency
404 of MOG_{38-49} tetramer-positive $CD4^+$ T cells. **h,** Quantification of the frequency and count of MOG_{38-}
405 $_{49}$ tetramer-positive $CD4^+$ T cells. For clinical scores and normalized weights, data represent mean
406 ± SEM. All other data represents mean ± SD.

407

408 **Fig.2 I OCA-B promotes Th1 and Th17 adoptive transfer EAE through recall response**

409 **a and b,** *Ocab*$^{fl/fl}$ and *Ocab*$^{fl/fl}$;CD4-Cre mice were primed with MOG_{35-55} peptide in CFA for 10-14
410 days. Cells from the spleens and lymph nodes of primed mice were isolated and cultured for 4
411 days in Th1 or Th17 polarizing conditions. $3.0x10^6$ Th1- or Th17-polarized cells were injected i.p.
412 into C57BL/6 wildtype recipient mice (Th1: *Ocab*$^{fl/fl}$ n=5, *Ocab*$^{fl/fl}$;CD4-Cre n=5) (Th17: *Ocab*$^{fl/fl}$
413 n=3, *Ocab*$^{fl/fl}$;CD4-Cre n=4). Clinical scores were assessed for 14-15 days. **c,** At Th17 adoptive
414 transfer EAE endpoint, brains and spinal cords were analyzed by flow cytometry. Quantification
415 of brain- and spinal cord-infiltrating $CD4^+$ T cells following Th17 adoptive transfer. **d,**
416 Representative flow cytometry plots showing the frequency of IFNγ and IL-17 expressing $CD4^+$ T
417 cells within the spines of Th17 recipient mice. **e,** Quantification of IL-17 frequency in spinal cord
418 infiltrating $CD4^+$ T cells. **f,** Schematic of in vitro Th17 differentiation restimulation assay. **g,** Naïve
419 $CD4^+$ T cells were initially stimulated with αCD3 and αCD28 for 2 days during Th17 differentiation
420 then restimulated after resting for 8 days. Representative flow cytometry plots showing frequency
421 of IFNγ and IL-17 expressing $CD4^+$ T cells after restimulation. **h,** Quantification of IFNγ and IL-17
422 expressing $CD4^+$ T cells following restimulation. For clinical scores, data represent mean ± SEM.
423 All other data represents mean ± SD.

424

425

426 **Fig.3 l OCA-B is dispensable for T cell response to CNS infection with a neurotropic virus**

427 **a,** *Ocab*$^{fl/fl}$ (n=6) and *Ocab*$^{fl/fl}$;CD4-Cre (n=6) mice were injected intracranially with 1500 PFU
428 JHMV. Clinical scores were recorded for 21 days post infection (dpi). **b,** Representative H&E/LFB
429 staining of spinal cord sections at 12 and 21 dpi. Demyelinated areas are outlined in black. **c,**
430 Quantification of % demyelination in spinal cord sections. Half brains were taken at 7, 12, and 21
431 dpi for flow cytometric and viral titer analysis. **d,** Quantification of CD4$^+$ T cell counts within half
432 brain. **e,** Representative plots showing the frequency of IFNγ expressing CD4$^+$ T cells 7, 12, and
433 21 dpi. **f,** Quantification of frequency of IFNγ expressing CD4$^+$ T cells. **g,** Half brain viral titers at
434 dpi 7, 12, and 21 (n.d., not detected). For clinical scores, data represent mean ± SEM. All other
435 data represents mean ± SD.

436

437 **Fig.4 l OCA-B expression marks encephalitogenic stem-like CD4$^+$ T cells**

438 **a,** OCA-B-mCherry mice were injected with MOG$_{35-55}$ peptide in CFA and *pertussis* toxin to induce
439 EAE. Cervical lymph nodes (CLNs), brains, and spines were isolated at peak disease (day 15)
440 and analyzed by flow cytometry for mCherry, CD44 and CD62L expression. **b,** CD44 and CD62L
441 expressing CD4$^+$ T cells were quantified based on mCherry expression. **c,** OCA-B-mCherry mice
442 were injected with MOG$_{35-55}$ peptide in CFA for 14 days. CD4$^+$ T cells within CLNs and spleens
443 were profiled by flow cytometry for mCherry, CD44, and CD62L expression. **d,** Quantification of
444 CD44 and CD62L expression of OCA-B negative and positive CD4$^+$ T cells from MOG-primed
445 OCA-B-mCherry mice. **e,** Bulk RNA sequencing was performed on OCA-B positive and negative
446 CD4$^+$ T cells from MOG$_{35-55}$ primed OCA-B-mCherry reporter mice. Heatmap showing relative
447 expression of the top 40 differentially expressed genes from OCA-B positive and negative CD4$^+$
448 T cells. **f,** Volcano plot of differentially expressed genes between OCA-B positive and negative T
449 cells (p value > 0.05 and Log2 fold change > 1 are colored). **g,** Gene Ontology (GO) terms
450 associated with OCA-B positive and negative groups. (**H**) EAE clinical scores of C57BL/6 wild-
451 type mice after receiving OCA-B positive or negative Th1 polarized CD4$^+$ T cells. For Clinical
452 scores, data represents mean ± SEM. All other data represents mean ± SD.

453

454 **Fig.5 l OCA-B promotes relapsing-remitting EAE through stem-like CD4$^+$ T cells**

455 **a,** NOD.*Ocab*$^{fl/fl}$ (n=19) and NOD.*Ocab*$^{fl/fl}$;CD4-Cre (n=15) mice were injected with MOG$_{35-55}$
456 peptide in CFA and *pertussis* toxin to induce EAE. Clinical scores of animals representing

457 relapsing-remitting disease progression over time. **b,** Animal weights were recorded to determine
458 weight loss throughout initial disease and relapse. **c,** Singe cell RNA sequencing was performed
459 on pooled CD3ε$^+$ cells isolated from the brain and spine of NOD.*Ocab*$^{fl/fl}$ (n=3) and
460 NOD.*Ocab*$^{fl/fl}$;CD4-Cre (n=4) 24 days after EAE induction (remission timepoint). Cell populations
461 were plotted in a UMAP using the Seurat R package and percentages are shown for each cluster.
462 Clusters were identified through differential gene expression analysis. **d,** Feature plots comparing
463 the expression of *Foxp3* and *Mki67* amongst clusters. **e,** Violin plots showing the expression of
464 *Btg1*, *Samhd1*, *Slamf6*, *Tcf7, Sell* and *Tox* within the Treg, proliferating, and Th1-like clusters. **f,**
465 CNS cells isolated at remission timepoint (day 24) were analyzed by spectral cytometry.
466 Representative flow cytometry plots and quantification showing the frequency of CD4$^+$ T cells
467 between control and experimental groups. **g,** Representative flow cytometry plots and
468 quantification showing the frequency of CXCR6 expressing CD4$^+$ T cells. **h,** Representative flow
469 cytometry plots showing the frequency of CD4$^+$ T cells expressing IFNγ and GM-CSF. **i,**
470 Quantification of CD4$^+$ T cells expressing IFNγ and GM-CSF. For clinical scores, data represents
471 mean ± SEM. All other data represents mean ± SD.
472
473 **Fig.6 I OCA-B promotes disease relapse through control of pathogenic stem-like Th17**
474 **differentiation**
475 **a,** Singe cell RNA and TCR sequencing were performed on pooled CD3ε$^+$ cells isolated from the
476 brain and spine of NOD.*Ocab*$^{fl/fl}$ (n=5) and NOD.*Ocab*$^{fl/fl}$;CD4-Cre (n=6) 33 days after EAE
477 induction (relapse timepoint). Cell populations were plotted in a UMAP using the Seurat R
478 package and percentages are shown for each cluster. Clusters were identified through differential
479 gene expression analysis. **b,** UMAP TCR clonotype expansion between *Ocab*$^{fl/fl}$ and *Ocab*$^{fl/fl}$;CD4-
480 Cre amongst clusters. **c,** Violin plots showing expression of *Ccr9*, *Bach2*, *Ccr7*, *Tcf7*, *Cd44*, *Cxcr6*,
481 *Il1r1* and *Lgals3* in the Ccr9 Stem-like CD4, Stem-like CD4-2, and Th17-like clusters. **d,** Feature
482 plots comparing the expression of *Ccr9*, *Tcf7*, and *Bach2* amongst clusters. **e,** UMAPs showing
483 RNA velocity of spliced and unspliced transcripts by experimental condition. **f,** Violin plots showing
484 expression of *Pdcd1*, *Tigit*, and *Il1r1* in the Th17-like cluster between control and experimental
485 groups.
486

487 **Extended data legends**

488 **Extended Data Fig.1. Minimal differences in cytokine expressing CD4$^+$ T cell, CD8$^+$ T cell,**
489 **B cell, macrophage or microglial cell counts at peak chronic EAE in OCA-B knockouts**

490 **a,** Quantification of frequency and count of CD8α positive T cells between Ocab$^{fl/fl}$ and
491 Ocab$^{fl/fl}$;CD4-Cre mice. **b,** Quantification of the number of B cells, macrophages and microglia. **c,**
492 Quantification of frequency and count of IFNγ, IL-17, and GM-CSF expressing CD4$^+$ T cells from
493 Ocab$^{fl/fl}$ and Ocab$^{fl/fl}$;CD4-Cre mice. All data represents mean $\pm$ SD.

494

495 **Extended Data Fig.2. Loss of OCA-B does not strongly alter initial Th1 or Th17 polarization**
496 **in vitro**

497 **a,** Representative flow cytometry plots showing IFNγ and IL-17 expressing CD4$^+$ T cells after
498 Th1 *in vitro* polarization. **b,** Quantification of IFNγ expressing CD4$^+$ T cells after Th1 polarization.
499 **c,** Representative flow cytometry plots showing IFNγ and IL-17 expressing CD4$^+$ T cells after
500 Th17 *in vitro* polarization. **d,** Quantification of IL-17 expressing CD4$^+$ T cells after Th17
501 polarization. All data represents mean $\pm$ SD.

502

503 **Extended Data Fig.3. Normal immune responses to intracranial JHMV infection in the**
504 **absence of OCA-B**

505 **a,** Quantification of the number of IFNγ expressing CD4$^+$ T cells at dpi 7, 12 and 21. **b,**
506 Quantification of the number of CD8$^+$ T cells at dpi 7, 12 and 21. **c,** Quantification of the
507 frequency of IFNγ expressing CD8$^+$ T cells at dpi 7, 12 and 21. **d,** Quantification of the number
508 of IFNγ expressing CD8$^+$ T cells at dpi 7, 12 and 21. All data represents mean $\pm$ SD.

509

510 **Extended Data Fig.4. Sorting OCA-B-mCherry reporter T cells and additional analysis of**
511 **the effects of transferring OCA-B^{hi} versus OCA-B^{lo} CD4$^+$ cells**

512 **a,** Gating strategy for sorting of OCA-B$^+$ and OCA-B$^-$ CD4$^+$ T cells. **b,** Normalized weights of
513 NOD.Ocab$^{fl/fl}$ and NOD.Ocab$^{fl/fl}$;CD4-Cre mice following EAE induction. Normalized weight is
514 represented by mean $\pm$ SEM.

515

516 **Extended Data Fig.5. Individual NOD mouse EAE clinical scores, additional remission**
517 **scRNA-seq cluster annotation genes, and heat map of gene enrichments by cluster**

518 **a,** Clinical scores of individual NOD.Ocab$^{fl/fl}$ mice following EAE induction. **b,** Clinical scores of
519 individual NOD.Ocab$^{fl/fl}$;CD4-Cre mice following EAE induction. **c,** UMAP feature plots showing
520 expression of *Cxcr6*, *Il23r*, and *Bach2* amongst clusters at remission timepoint. **d,** Heatmap
521 showing the top 10 genes expressed by cluster at remission EAE timepoint.
522
523 **Extended Data Fig.6. Heat map of NOD.EAE relapse gene enrichments by cluster, TCR**
524 **clonotype overlap between condition, example relapse feature plots, and pseudotime**
525 **analysis of relapse single cell RNA seq**
526 **a,** Heatmap showing the top 10 genes expressed by cluster at relapse EAE timepoint. **b,** Alluvial
527 plot showing top 10 TCR clonotype gene overlap between Ocab$^{fl/fl}$ and Ocab$^{fl/fl}$;CD4-Cre groups.
528 **c,** UMAP feature showing the expression of *CD4*, *CD8a, Tox*, *Sell*, *Ccr7*, and *Ccr4* amongst
529 clusters at relapse timepoint. **d,** Pseudotime analysis of relapse single cell from root starting
530 node at or near Ccr9 stem-like cluster.
531
532 **Extended Data Fig.7. OCA-B promotes pathogenic maturation of stem-like Th17 cells in**
533 **EAE**
534 OCA-B expression promotes and selectively labels pathogenic stem-like Th17 cells which
535 preferentially transfer EAE and instigate disease relapse.

536 **Methods**

537 **Chronic C57BL/6 EAE**

538 11-12 week-old female C57BL/6 littermate animals were used for all experiments. For adoptive
539 transfer experiments using the OCA-B-mCherry reporter allele[47], 11 week-old females were used
540 for chronic EAE and 9 week-old males were used as MOG_{35-55} primed adoptive transfer donors.
541 EAE was induced on day 0 by two 100 μL subcutaneous injections into both hind flanks of 0.5
542 μmol/mL MOG_{35-55} peptide (University of Utah Peptide Core) emulsified in complete Freud's
543 adjuvant (CFA), comprised of incomplete Freund's adjuvant (Cat# 77145;ThermoFisher) together
544 with 4 mg/mL heat-killed *M. tuberculosis* (Cat# DF3114338; Fisher Scientific). Animals were given
545 two 400 ng intraperitoneal injections of *B. pertussis* toxin (Cat# 181; List Biological Laboratories)
546 on days 0 and 2.

547

548 **Clinical Scoring**

549 EAE clinical scores were determined using a 0-5 scale with 0.5 scoring intervals: 0.5, tip of tail is
550 limp or tail muscle strain observed; 1, complete limp tail; 1.5, complete limp tail and at least one
551 hind limb consistently falls through wire rack when animal is dropped; 2, complete limp tail and
552 one hind leg dragging without movement beyond hip; 2.5, complete limp tail and dragging of both
553 hind limbs without movement beyond hip; 3, complete hind limb paralysis; 3.5, complete hind limb
554 paralysis with flat laying hind quarters and hump in upper torso; 4, complete hind limb and partial
555 forelimb paralysis, minimal movement around cage; 4.5, complete hind limb and partial forelimb
556 paralysis, no movement around cage; 5, seizure or death. Animals scoring a ≥4 for more than 48
557 hr were euthanized and scored 5 for the remainder of the experiment. JHMV clinical disease was
558 evaluated using previously described 0-4 point scale[66].

559

560 **Histology**

561 Spinal columns were isolated from C57BL/6 $Ocab^{fl/fl}$ and $Ocab^{fl/fl}$;CD4-Cre animals after EAE or
562 JHMV induced demyelination and fixed overnight in in 4% paraformaldehyde at 4C. Spinal cords
563 were subsequently isolated and cryoprotected in 30% sucrose for 3-5 days. Thoracic and lumbar
564 sections were embedded in optimum cutting temperature (OCT) compound (ThermoFisher
565 Scientific) and frozen and stored at -80C. 8 µm spinal sections were cut by cryostat and stained
566 with Luxol fast blue (Cat# 212170250; ThermoFisher) along with hematoxylin (Cat# 8495; ENG

567 Scientific) and eosin (Cat# E511-25; Fisher Chemical). Demyelination was assessed by dividing
568 the area of demyelinated white matter by total white matter as previously described[67,68].
569
570 **Flow cytometry and spectral cytometry.**
571 Spinal cords and brains were harvested at peak disease or specified timepoint and mechanically
572 dissociated by passing through a 100 µm cell strainer. A 30/70% Percoll gradient (Cat# 17544501;
573 Cytiva) was used to enrich mononuclear cells. Cells from collected spleens and lymph nodes
574 (cervical, brachial, axillary and inguinal) were passed through a 70 µm strainer and erythrocytes
575 lysed by ammonium-chloride-potassium lysis buffer (150 mM NH_4Cl, 10 mM $KHCO_3$, 0.1 mM
576 Na_2EDTA). For intracellular staining, cells were cultured in complete media (RPMI 1640, 10%
577 FBS, 1% Pen/Strep, Glutamax) supplemented with 1 µL/mL brefeldin A (Cat# 555029; Golgiplug,
578 BD), 50 ng/mL phorbol myristate acetate (Cat# P1585; Sigma-Aldrich) and 1 µg/mL ionomycin
579 (Cat# I0634; Sigma-Aldrich) for 4 hr. Cultured cells were fixed using cytofix/cytoperm (Cat#
580 554714; BD) according to manufacturer's protocol and stained for intracellular cytokines in
581 perm/wash buffer. Flow cytometry samples were profiled using a BD Fortessa (BD Biosciences,
582 Fig. 2, 3, 4) or an Aurora spectral flow cytometer (Cytek, Fig. 1, 5). FlowJo software (BD
583 Biosciences) was used for data analysis.
584
585 **Th1 and Th17 polarization and adoptive transfer C57BL/6 EAE**
586 10-12 week-old female C57BL/6 littermate animals were used for all experiments. Donor animals
587 were immunized with MOG_{35-55} in CFA as above. 10-14 days post-immunization, spleen and
588 lymph node (cervical, axillary, brachial and inguinal) cells were collected and placed into mixed
589 culture with MOG peptide and cytokines at 5.0×10^6 cells/mL. For Th1 conditions, complete media
590 was supplemented with 50 µg/mL MOG_{35-55}, 6 ng/mL rmIL-6 (Cat# 216-16; Peprotech) and 2
591 ng/mL rmIFNγ (Cat# 315-05; Peprotech). For Th17 conditions, complete media was
592 supplemented with 50 µg/mL MOG_{35-55}, 8 ng/mL rmIL-23 (Cat# 1887-ML-010; R&D Systems), 10
593 ng/mL rmIL-1α (Cat# 211-11A; Peprotech), and 10 µg/mL anti-IFNγ (Cat# BE0055; BioXcell
594 XMG1.2). After 4 days of respective culture, $CD4^+$ T cells were purified using negative magnetic
595 selection and resuspended in PBS at 1.5×10^6 cells/mL. 100uL cell suspension was injected
596 intraperitoneally into WT C57BL/6 recipients. Clinical disease was scored for 15 days.
597
598 **In vitro Th17 differentiation restimulation assay**

599 Naïve CD4+ T cells were isolated from *Ocab*$^{fl/fl}$ and *Ocab*$^{fl/fl}$;CD4-Cre C57BL/6 mice by magnetic
600 negative selection (Miltenyi Bio kit and LS columns). Naïve CD4+ T cells were cultured in anti-
601 CD3ε coated (10 µg/mL) 96-well plates (2.0x10^5 cells/well) with Th17 differentiation media and
602 soluble anti-CD28 (2 µg/mL). Th17 differentiation media consisted of complete media
603 supplemented with 2 µg/mL anti-IL-4 (Cat# 504101; Biolegend), 2 µg/mL anti-IFNγ (Cat# BE0055;
604 XMG 1.2, BioXcell), 20 ng/mL IL-6 (Peprotech), 5 ng/mL TGF-β (Peprotech), and 10 ng/mL IL-23
605 (R&D Systems). After 2 days, cells were replated into new 96-well plates with fresh Th17
606 differentiation media but lacking anti-CD3ε. On day 5, cells were resuspended in complete media.
607 On day 10, cells designated for restimulation were cultured for 12 hours in a new 96-well plate
608 coated with 10 µg/mL anti-CD3 in complete media supplemented with 2 µg/mL anti-CD28. Rested
609 and restimulated cells were analyzed by flow cytometry.
610
611 **JHMV**
612 *Ocab*$^{fl/fl}$ and *Ocab*$^{fl/fl}$;CD4-Cre C57BL/6 mice were anesthetized using isoflurane. Mice were
613 intracranially (i.c) injected with 1500 plaque-forming units (PFU) of JHMV (strain V34) suspended
614 in 30 µL Hank's balanced salt solution (ThermoFisher). Clinical disease was assessed for 21 days
615 using a previously described scale[69]. Mice were sacrificed at days 7, 12, and 21 post-infection to
616 assess viral titers within brain homogenates using a plaque assay previously described[70]. Spinal
617 cords were taken on day 21 post-infection to assess demyelination by luxol fast blue and
618 hematoxylin/eosin histology.
619
620 **OCA-B-mCherry adoptive transfer EAE**
621 OCA-B-mCherry reporter allele animals[47] were primed for 14 days with MOG_{35-55} in CFA as
622 described above. After priming, spleen and lymph nodes were collected and CD4+ T cells were
623 purified by magnetic negative selection (Miltenyi Bio kit and LS columns). Non-CD4+ T cells were
624 removed from the LS column and placed on ice for subsequent in vitro culture. Purified CD4+ T
625 cells were separated by OCA-B-mCherry expression (PE-Texas Red) using flow automated cell
626 sorting (FACS). OCA-B-mCherry positive and negative CD4+ T cells were placed into mixed
627 culture in complete medium with the previously purified non-CD4+ T cells at a 1:10 ratio (CD4+ to
628 non-CD4+) at 1.0×10^6 cells/mL. The culture was supplemented with 20 µg/mL MOG_{35-55} and 0.5
629 ng/mL IL-12p70 (Cat# 210-12; Peprotech). After two days of culture, CD4+ T cells were again
630 purified through negative magnetic selection. Purified CD4+ T cells from OCA-B-mCherry positive

631 and negative cultures were resuspended in PBS at 8.8×10^6 cells/mL. 100 µL cell suspension was
632 injected i.p. into age-matched male C57BL/6 recipients. Clinical disease was assessed for 24
633 days.
634
635 **Bulk RNAseq**
636 OCA-B-mCherry reporter mice (n=9) were primed for 14 days with MOG_{35-55} in CFA as described
637 above. After priming, lymph nodes (cervical, axillary, brachial and inguinal) were isolated and
638 mCherry positive and negative $CD4^+$ T cells were collected by FACS. Total RNA, three groups
639 (pooled 3 mice each), was isolated using the Quick RNA micro kit (Cat# R1050; Zymo Research)
640 with DNase treatment (Cat# 79254; Qiagen). RNA concentration was measured with a Qubit RNA
641 HS Assay Kit (Cat# #Q32855; Fisher Scientific). RNA quality was evaluated with an RNA
642 ScreenTape Assay (Cat# 5067-5579, 5067-5580; Agilent Technologies). Total RNA samples (5-
643 500 ng) were hybridized with NEBNext rRNA Depletion Kit v2 (Cat# E7400; New England Biolabs)
644 to diminish rRNA from the samples. Stranded RNA sequencing libraries were prepared as
645 described using the NEBNext Ultra II Directional RNA Library Prep Kit for Illumina (Cat# E7760L;
646 New England Biolabs). Purified libraries were qualified on an 4150 TapeStation (Agilent
647 Technologies) using a D1000 ScreenTape assay (Cat# 5567-5582, 5067-5583; Agilent
648 Technologies). The molarity of adapter-modified molecules was defined by quantitative PCR
649 using the Kapa Biosystems Kapa Library Quant Kit (Cat# KK4824Roche). Individual libraries were
650 normalized to 5 nM. NovaSeq 150×150 bp sequencing libraries were chemically denatured and
651 applied to an Illumina NovaSeq flow cell using the XP workflow (20043131). Following transfer to
652 an Illumina NovaSeq 6000 instrument, 150×150 cycle paired-end sequencing was performed
653 using a S4 reagent Kit v1.5 (Cat# 20028312; Illumina). 8-11 million reads were generated per
654 sample and were aligned to the *GRCm38* mouse reference genome. Differential gene expression
655 and pathway analysis were conducted using the DESeq2 and Enrichr R packages.
656
657 **NOD-EAE**
658 15-18 week-old female littermate *Ocab*$^{fl/fl}$ and *Ocab*$^{fl/fl}$;CD4-Cre animals backcrossed to a NOD
659 strain background[31] were used for all experiments. EAE was induced by two 100 µL subcutaneous
660 injections into both hind flanks of 0.5 µmol/mL MOG_{35-55} peptide emulsified in incomplete Freuds
661 adjuvant (Cat# 77145; ThermoFisher) supplemented with 4 mg/mL heat-killed *M. tuberculosis*
662 (Cat# DF3114338; Fisher Scientific) to form CFA. Animals were given two 400 ng intraperitoneal

663 injections of *Bordetella pertussis* toxin (Cat# 181; List Biological Laboratories) on days 0 and 2.
664 Clinical disease was assessed over 47 days using a 5-point scale described below. Remission
665 timepoints were determined to be between days 22-26 while relapse was determined to be
666 between days 26-39.
667
668 **Single-cell RNA-seq**
669 NOD.*Ocab*$^{fl/fl}$ and NOD.*Ocab*$^{fl/fl}$;CD4-Cre animals were induced with EAE and monitored for
670 disease progression. Brains and spinal cords were isolated on day 24 (remission) and day 33
671 (relapse), and processed for FACS sorting. Viable cells were sorted by CD3ε using a FACSAria
672 (BD Bioscience). Cells from each condition were isolated from 3-4 mice and combined. Cells were
673 processed using the 5' 10X Genomics Chromium platform according to the manufacturer's
674 instructions. Paired-end high-throughput sequencing (125 cycles) was performed using a
675 NovaSeq instrument (Illumina). Sequencing reads were processed by using the 10X Genomics
676 CellRanger pipeline and further analyzed using the Seurat R package. Analysis of cells used a
677 standard filtering protocol removing cells with unique feature counts of >5,000 or <100, as well as
678 cells with >10% mitochondrial counts (indicative of dead cells). No more than 10% of total cells
679 were removed by this process. Cells were subjected to unsupervised hierarchical clustering
680 followed by uniform manifold approximation and projection (UMAP) to visualize clusters with
681 similar gene expression and their relative positions. RNA velocity analysis was performed using
682 velocyto.R version 0.6 to model cell state transitions using the guidelines provided in Manno et
683 al.[49] and the associated repository at https://github.com/velocyto-team/velocyto.R. High
684 dimensional velocity vectors were graphed on the predefined Seurat UMAP projection using
685 localized average grid projections. Pseudotime analysis was conducted using Seurat and
686 Monocle3 packages. Integrated data was divided into subset based on genotype and Monocle3
687 was used to calculate trajectory, order cells and plot pseudotime for each condition.
688
689 **Statistics**
690 Multiple two-tailed student's t-tests were used to determine statistical differences in EAE clinical
691 scores and all error bars denote ±SEM unless otherwise noted. Two-way ANOVA statistical tests
692 were used to determine differences in weight loss throughout disease progression. GraphPad
693 Prism software was used for all statistics and graphing. Two-tailed student's t-tests were used to
694 determine statistical differences in cell populations observed by flow cytometry and all error bars

represent ± SD unless otherwise noted. For all figures, ns = $p>0.05$, * = $p\leq0.05$, ** = $p\leq0.01$, *** = $p\leq0.001$, **** = $p\leq0.0001$.

697 **Reporting summary**

698 Information regarding research design is available in the Nature Portfolio Reporting Summary
699 linked to this article.

700

701 **Data availability**

702 All RNA sequencing, single-cell sequencing, and single-cell T cell V(D)J sequencing data
703 associated with the findings of this study have been deposited to NCBI's GEO database under
704 accession code GSE243727.

705

706 **Acknowledgements**

707 We thank R.M. O'Connell and M. Bettini for critical reading of the manuscript. We thank J. Marvin
708 and University of Utah Health Sciences Center Flow Cytometry core, and B. Dalley, O. Allen and
709 the High-Throughput Genomics core. Peptides were synthesized by the DNA/Peptide facility. We
710 thank T. Lane for assistance with JHMV constructs, protocols and reagents. This work was
711 supported by grants from the National Institutes of Health/ National Institute of Allergy and
712 Infectious Diseases (R01AI162929 and R01AI100873) and the Praespero Foundation (Canada)
713 to DT, and the National Institute of Neurological Disorders and Stroke (T32NS115664) to EPH.

714

715 **Author contributions**

716 E.P.H. and D.T. conceived the study. E.P.H. and A.S. performed experiments. E.P.H, A.S.,
717 E.M.M. and B.T.S. analyzed data. T.E.L., B.T.S. and D.T. provided critical resources and
718 supervision for the study. E.P.H. and D.T. wrote, reviewed and revised the manuscript.

719

720 **Competing interests**

721 The authors declare that they have no conflicts of interest

722 **References**

723 1. Wallin, M. T. *et al.* The prevalence of MS in the United States. *Neurology* **92**, e1029–
724 e1040 (2019).
725 2. Wtccc, C. C. *et al.* Genetic risk and a primary role for cell-mediated immune mechanisms
726 in multiple sclerosis. *Nature* **476**, 214–219 (2011).
727 3. IMSGC. A high-density screen for linkage in multiple sclerosis. *Am. J. Hum. Genet.* **77**,
728 454–467 (2005).
729 4. Adorini, L., Guery, J.-C. & Trembleau, S. Manipulation of the Th1/Th2 Cell Balance: An
730 Approach to Treat Human Autoimmune Diseases? *Autoimmunity* **23**, 53–68 (1996).
731 5. Langrish, C. L. *et al.* IL-23 drives a pathogenic T cell population that induces autoimmune
732 inflammation. *J. Exp. Med.* **201**, 233–240 (2005).
733 6. Brucklacher-Waldert, V., Stuerner, K., Kolster, M., Wolthausen, J. & Tolosa, E.
734 Phenotypical and functional characterization of T helper 17 cells in multiple sclerosis.
735 *Brain* **132**, 3329–3341 (2009).
736 7. Montes, M. *et al.* Oligoclonal myelin-reactive T-cell infiltrates derived from multiple
737 sclerosis lesions are enriched in Th17 cells. *Clin. Immunol.* **130**, 133–144 (2009).
738 8. Hartmann, F. J. *et al.* Multiple sclerosis-associated IL2RA polymorphism controls GM-
739 CSF production in human TH cells. *Nat. Commun.* **5**, 5056 (2014).
740 9. Scholz, C., Patton, K. T., Anderson, D. E., Freeman, G. J. & Hafler, D. A. Expansion of
741 Autoreactive T Cells in Multiple Sclerosis Is Independent of Exogenous B7 Costimulation.
742 *J. Immunol.* **160**, 1532–1538 (1998).
743 10. Burns, J. B., Bartholomew, B. D. & Lobo, S. T. Isolation of CD45RO+, Memory T Cells
744 Recognizing Proteolipid Protein from Neurologically Normal Subjects. *Cell. Immunol.* **212**,
745 44–50 (2001).
746 11. Pelfrey, C. M. *et al.* Quantification of Self-Recognition in Multiple Sclerosis by Single-Cell
747 Analysis of Cytokine Production. *J. Immunol.* **165**, 1641–1651 (2000).
748 12. Lovett-Racke, A. E. *et al.* Decreased dependence of myelin basic protein-reactive T cells
749 on CD28-mediated costimulation in multiple sclerosis patients. A marker of
750 activated/memory T cells. *J. Clin. Invest.* **101**, 725–730 (1998).
751 13. Lee, H.-G. *et al.* Pathogenic function of bystander-activated memory-like CD4+ T cells in
752 autoimmune encephalomyelitis. *Nat. Commun.* **10**, 709 (2019).
753 14. Williams, J. L. *et al.* Memory cells specific for myelin oligodendrocyte glycoprotein (MOG)
754 govern the transfer of experimental autoimmune encephalomyelitis. *J. Neuroimmunol.*

755 **234**, 84–92 (2011).
756 15. Elyaman, W. *et al.* Distinct Functions of Autoreactive Memory and Effector CD4+ T Cells
757 in Experimental Autoimmune Encephalomyelitis. *Am. J. Pathol.* **173**, 411–422 (2008).
758 16. Maurano, M. T. *et al.* Systematic Localization of Common Disease-Associated Variation
759 in Regulatory DNA. *Science (80-.).* **337**, 1190–1195 (2012).
760 17. Graham, D. S. C., Wong, A. K., McHugh, N. J., Whittaker, J. C. & Vyse, T. J. Evidence for
761 unique association signals in SLE at the CD28–CTLA4–ICOS locus in a family-based
762 study. *Hum. Mol. Genet.* **15**, 3195–3205 (2006).
763 18. van Heel, D. A. Inflammatory bowel disease is associated with a TNF polymorphism that
764 affects an interaction between the OCT1 and NF-kappaB transcription factors. *Hum. Mol.*
765 *Genet.* **11**, 1281–1289 (2002).
766 19. Farh, K. K. *et al.* Genetic and epigenetic fine mapping of causal autoimmune disease
767 variants. *Nature* **518**, 337–343 (2015).
768 20. Kim, H. *et al.* T cell-selective deletion of Oct1 protects animals from autoimmune
769 neuroinflammation while maintaining neurotropic pathogen response. *J.*
770 *Neuroinflammation* **16**, 133 (2019).
771 21. Hwang, S. S., Kim, L. K., Lee, G. R. & Flavell, R. A. Role of OCT-1 and partner proteins
772 in T cell differentiation. *Biochim. Biophys. Acta - Gene Regul. Mech.* **1859**, 825–831
773 (2016).
774 22. Kim, L. K. *et al.* Oct-1 Regulates IL-17 Expression by Directing Interchromosomal
775 Associations in Conjunction with CTCF in T Cells. *Mol. Cell* **54**, 56–66 (2014).
776 23. Shakya, A. *et al.* Oct1 and OCA-B are selectively required for CD4 memory T cell
777 function. *J. Exp. Med.* **212**, 2115–2131 (2015).
778 24. Vázquez-Arreguín, K. *et al.* Oct1/Pou2f1 is selectively required for colon regeneration and
779 regulates colon malignancy. *PLOS Genet.* **15**, e1007687 (2019).
780 25. Perovanovic, J. *et al.* Oct1 cooperates with the Smad family of transcription factors to
781 promote mesodermal lineage specification. *Sci. Signal.* **16**, (2023).
782 26. Sebastiano, V. *et al.* Oct1 regulates trophoblast development during early mouse
783 embryogenesis. *Development* **137**, 3551–3560 (2010).
784 27. Hwang, S. S., Kim, L. K., Lee, G. R. & Flavell, R. A. Role of OCT-1 and partner proteins
785 in T cell differentiation. *Biochim. Biophys. Acta - Gene Regul. Mech.* **1859**, 825–831
786 (2016).
787 28. Kim, U. *et al.* The B-cell-specific transcription coactivator OCA-B/OBF-1/Bob-1 is

788 essential for normal production of immunoglobulin isotypes. *Nature* **383**, 542–547 (1996).
789 29. The GAMES Collaborative Group. Linkage disequilibrium screening for multiple sclerosis
790 implicates JAG1 and POU2AF1 as susceptibility genes in Europeans. *J. Neuroimmunol.*
791 **179**, 108–116 (2006).
792 30. Nakamura, M. *et al.* Genome-wide Association Study Identifies TNFSF15 and POU2AF1
793 as Susceptibility Loci for Primary Biliary Cirrhosis in the Japanese Population. *Am. J.*
794 *Hum. Genet.* **91**, 721–728 (2012).
795 31. Kim, H. *et al.* Targeting transcriptional coregulator OCA-B/Pou2af1 blocks activated
796 autoreactive T cells in the pancreas and type 1 diabetes. *J. Exp. Med.* **218**, 133 (2021).
797 32. Tzartos, J. S. *et al.* IL-21 and IL-21 Receptor Expression in Lymphocytes and Neurons in
798 Multiple Sclerosis Brain. *Am. J. Pathol.* **178**, 794–802 (2011).
799 33. Ndhlovu, L. C., Ishii, N., Murata, K., Sato, T. & Sugamura, K. Critical Involvement of
800 OX40 Ligand Signals in the T Cell Priming Events During Experimental Autoimmune
801 Encephalomyelitis. *J. Immunol.* **167**, 2991–2999 (2001).
802 34. Hurwitz, A. A., Sullivan, T. J., Sobel, R. A. & Allison, J. P. Cytotoxic T lymphocyte
803 antigen-4 (CTLA-4) limits the expansion of encephalitogenic T cells in experimental
804 autoimmune encephalomyelitis (EAE)-resistant BALB/c mice. *Proc. Natl. Acad. Sci.* **99**,
805 3013–3017 (2002).
806 35. Arellano, G., Ottum, P. A., Reyes, L. I., Burgos, P. I. & Naves, R. Stage-Specific Role of
807 Interferon-Gamma in Experimental Autoimmune Encephalomyelitis and Multiple
808 Sclerosis. *Front. Immunol.* **6**, (2015).
809 36. Rottman, J. B. *et al.* The costimulatory molecule ICOS plays an important role in the
810 immunopathogenesis of EAE. *Nat. Immunol.* **2**, 605–611 (2001).
811 37. Rouse, M., Nagarkatti, M. & Nagarkatti, P. S. The role of IL-2 in the activation and
812 expansion of regulatory T-cells and the development of experimental autoimmune
813 encephalomyelitis. *Immunobiology* **218**, 674–682 (2013).
814 38. Duncker, P. C., Stoolman, J. S., Huber, A. K. & Segal, B. M. GM-CSF Promotes Chronic
815 Disability in Experimental Autoimmune Encephalomyelitis by Altering the Composition of
816 Central Nervous System–Infiltrating Cells, but Is Dispensable for Disease Induction. *J.*
817 *Immunol.* **200**, 966–973 (2018).
818 39. Yosef, N. *et al.* Dynamic regulatory network controlling TH17 cell differentiation. *Nature*
819 **496**, 461–468 (2013).
820 40. Ikegami, I., Takaki, H., Kamiya, S., Kamekura, R. & Ichimiya, S. Bob1 enhances RORγt-

821 mediated IL-17A expression in Th17 cells through interaction with RORγt. *Biochem.*
822 *Biophys. Res. Commun.* **514**, 1167–1171 (2019).
823 41. Baker, D. *et al.* Autoimmune encephalomyelitis in NOD mice is not initially a progressive
824 multiple sclerosis model. *Ann. Clin. Transl. Neurol.* **6**, acn3.792 (2019).
825 42. Rumble, J. M. *et al.* Neutrophil-related factors as biomarkers in EAE and MS. *J. Exp.*
826 *Med.* **212**, 23–35 (2015).
827 43. Kroenke, M. A., Carlson, T. J., Andjelkovic, A. V. & Segal, B. M. IL-12– and IL-23–
828 modulated T cells induce distinct types of EAE based on histology, CNS chemokine
829 profile, and response to cytokine inhibition. *J. Exp. Med.* **205**, 1535–1541 (2008).
830 44. Grifka-Walk, H. M., Lalor, S. J. & Segal, B. M. Highly polarized Th17 cells induce EAE via
831 a T-bet independent mechanism. *Eur. J. Immunol.* **43**, 2824–2831 (2013).
832 45. Shakya, A., Kang, J., Chumley, J., Williams, M. A. & Tantin, D. Oct1 Is a Switchable,
833 Bipotential Stabilizer of Repressed and Inducible Transcriptional States. *J. Biol. Chem.*
834 **286**, 450–459 (2011).
835 46. Murayama, A. *et al.* A specific CpG site demethylation in the human interleukin 2 gene
836 promoter is an epigenetic memory. *EMBO J.* **25**, 1081–1092 (2006).
837 47. Sun, W. *et al.* OCA-B / Pou2af1 is sufficient to promote CD4 + T cell memory and
838 prospectively identifies memory precursors. *BioRxiv* (2023).
839 doi:https://doi.org/10.1101/2022.09.21.508912
840 48. Schnell, A. *et al.* Stem-like intestinal Th17 cells give rise to pathogenic effector T cells
841 during autoimmunity. *Cell* **184**, 6281-6298.e23 (2021).
842 49. La Manno, G. *et al.* RNA velocity of single cells. *Nature* **560**, 494–498 (2018).
843 50. Schubart, D. B., Rolink, A., Kosco-Vilbois, M. H., Botteri, F. & Matthias, P. B-cell-specific
844 coactivator OBF-1/OCA-B/Bob1 required for immune response and germinal centre
845 formation. *Nature* **383**, 538–42 (1996).
846 51. Schubart, D. B., Rolink, A., Kosco-Vilbois, M. H., Botteri, F. & Matthias, P. B-cell-specif ic
847 coactivator OBF-1/OCA-B/Bob1 required for immune response and germinal centre
848 formation. *Nature* **383**, 538–542 (1996).
849 52. Qin, X. F., Reichlin, A., Luo, Y., Roeder, R. G. & Nussenzweig, M. C. OCA-B integrates B
850 cell antigen receptor-, CD40L- and IL 4-mediated signals for the germinal center pathway
851 of B cell development. *EMBO J.* **17**, 5066–75 (1998).
852 53. Heng, T. S. P. *et al.* The Immunological Genome Project: networks of gene expression in
853 immune cells. *Nat. Immunol.* **9**, 1091–1094 (2008).

854 54. Zwilling, S., Dieckmann, A., Pfisterer, P., Angel, P. & Wirth, T. Inducible Expression and
855 Phosphorylation of Coactivator BOB.1/OBF.1 in T Cells. *Science (80-.).* **277**, 221–225
856 (1997).
857 55. Gearty, S. V. *et al.* An autoimmune stem-like CD8 T cell population drives type 1
858 diabetes. *Nature* **602**, 156–161 (2022).
859 56. Paroni, M. *et al.* Recognition of viral and self-antigens by T H 1 and T H 1/T H 17 central
860 memory cells in patients with multiple sclerosis reveals distinct roles in immune
861 surveillance and relapses. *J. Allergy Clin. Immunol.* **140**, 797–808 (2017).
862 57. McRae, B. L. *et al.* Induction of active and adoptive relapsing experimental autoimmune
863 encephalomyelitis (EAE) using an encephalitogenic epitope of proteolipid protein. *J.*
864 *Neuroimmunol.* **38**, 229–240 (1992).
865 58. Bernard, C. C. A. *et al.* Myelin oligodendrocyte glycoprotein: a novel candidate
866 autoantigen in multiple sclerosis. *J. Mol. Med.* **75**, 77–88 (1997).
867 59. Anderson, A. C. *et al.* A Transgenic Model of Central Nervous System Autoimmunity
868 Mediated by CD4+ and CD8+ T and B Cells. *J. Immunol.* **188**, 2084–2092 (2012).
869 60. Nish, S. A. *et al.* CD4+ T cell effector commitment coupled to self-renewal by asymmetric
870 cell divisions. *J. Exp. Med.* **214**, 39–47 (2017).
871 61. Mammadli, M., Suo, L., Sen, J. M. & Karimi, M. TCF-1 Is Required for CD4 T Cell
872 Persistence Functions during AlloImmunity. *Int. J. Mol. Sci.* **24**, 4326 (2023).
873 62. Kadowaki, A., Saga, R., Lin, Y., Sato, W. & Yamamura, T. Gut microbiota-dependent
874 CCR9+CD4+ T cells are altered in secondary progressive multiple sclerosis. *Brain* **142**,
875 916–931 (2019).
876 63. Thakore, P. I. *et al.* The chromatin landscape of Th17 cells reveals mechanisms of
877 diversification of regulatory and pro-inflammatory states. *BioRxiv* (2022).
878 64. Song, S. *et al.* OBF1 and Oct factors control the germinal center transcriptional program.
879 *Blood* **137**, 2920–2934 (2021).
880 65. Sha, Y. & Markovic-Plese, S. Activated IL-1RI Signaling Pathway Induces Th17 Cell
881 Differentiation via Interferon Regulatory Factor 4 Signaling in Patients with Relapsing-
882 Remitting Multiple Sclerosis. *Front. Immunol.* **7**, (2016).
883 66. Lane, T. E. *et al.* A Central Role for CD4 + T Cells and RANTES in Virus-Induced Central
884 Nervous System Inflammation and Demyelination. *J. Virol.* **74**, 1415–1424 (2000).
885 67. Blanc, C. A. *et al.* Sphingosine-1-Phosphate Receptor Antagonism Enhances
886 Proliferation and Migration of Engrafted Neural Progenitor Cells in a Model of Viral-

887 Induced Demyelination. *Am. J. Pathol.* **185**, 2819–2832 (2015).
888 68. Plaisted, W. C. *et al.* Remyelination Is Correlated with Regulatory T Cell Induction
889 Following Human Embryoid Body-Derived Neural Precursor Cell Transplantation in a
890 Viral Model of Multiple Sclerosis. *PLoS One* **11**, e0157620 (2016).
891 69. Lane, T. E. *et al.* A central role for CD4(+) T cells and RANTES in virus-induced central
892 nervous system inflammation and demyelination. *J. Virol.* **74**, 1415–24 (2000).
893 70. Dickey, L. L., Worne, C. L., Glover, J. L., Lane, T. E. & O'Connell, R. M. MicroRNA-155
894 enhances T cell trafficking and antiviral effector function in a model of coronavirus-
895 induced neurologic disease. *J. Neuroinflammation* **13**, 240 (2016).
896

Fig. 1

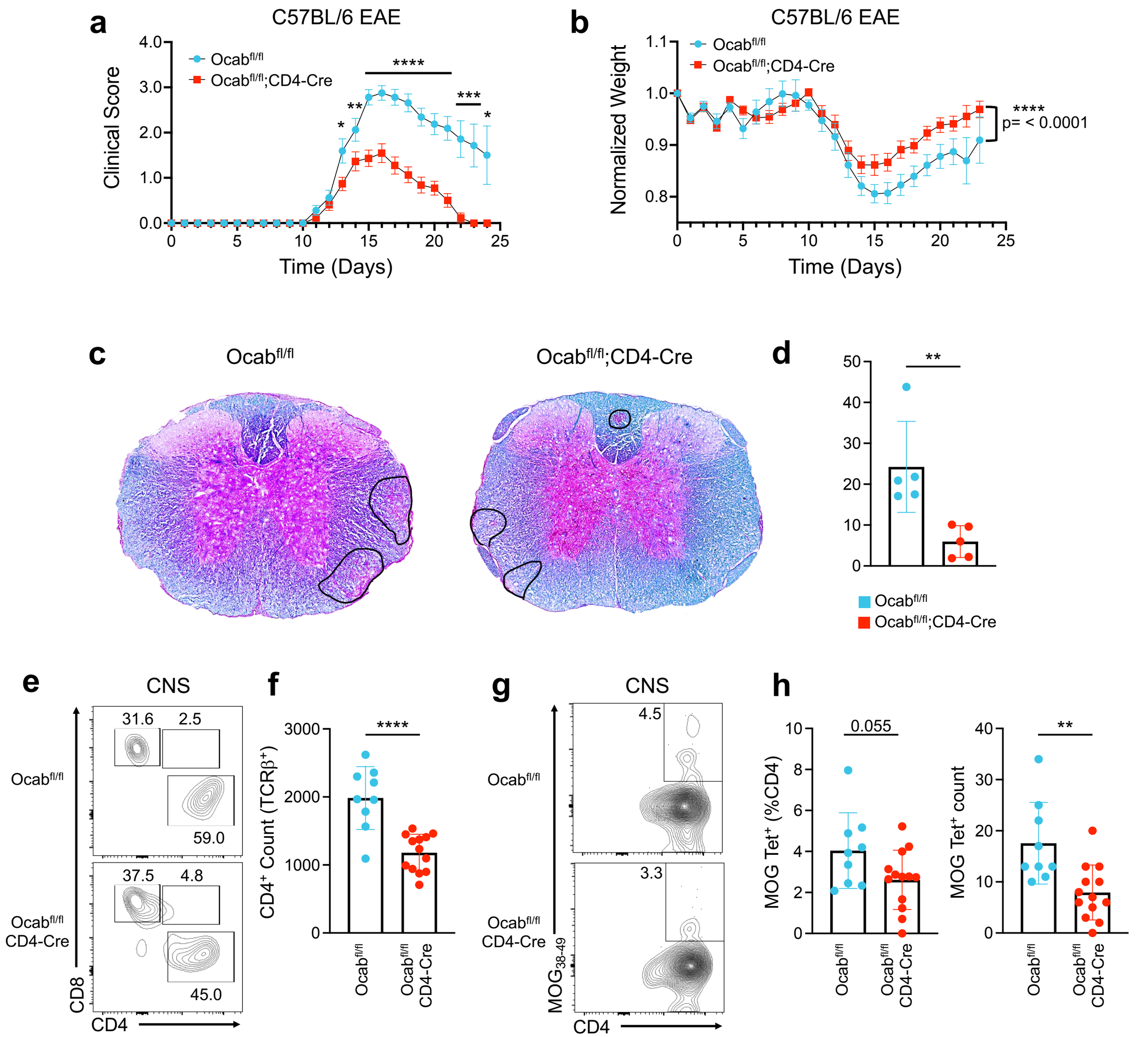
a
C57BL/6 EAE
Clinical Score
Time (Days)
Ocab$^{fl/fl}$
Ocab$^{fl/fl}$;CD4-Cre
****
***
**
*
b
C57BL/6 EAE
Normalized Weight
Time (Days)
Ocab$^{fl/fl}$
Ocab$^{fl/fl}$;CD4-Cre
****
p= < 0.0001
c
Ocab$^{fl/fl}$
Ocab$^{fl/fl}$;CD4-Cre
d
**
Ocab$^{fl/fl}$
Ocab$^{fl/fl}$;CD4-Cre
e
CNS
Ocab$^{fl/fl}$
Ocab$^{fl/fl}$ CD4-Cre
31.6
2.5
59.0
37.5
4.8
45.0
CD8
CD4
f
****
CD4$^+$ Count (TCRβ$^+$)
Ocab$^{fl/fl}$
Ocab$^{fl/fl}$ CD4-Cre
g
CNS
Ocab$^{fl/fl}$
Ocab$^{fl/fl}$ CD4-Cre
4.5
3.3
MOG$_{38-49}$
CD4
h
0.055
**
MOG Tet$^+$ (%CD4)
MOG Tet$^+$ count
Ocab$^{fl/fl}$
Ocab$^{fl/fl}$ CD4-Cre

Fig. 2

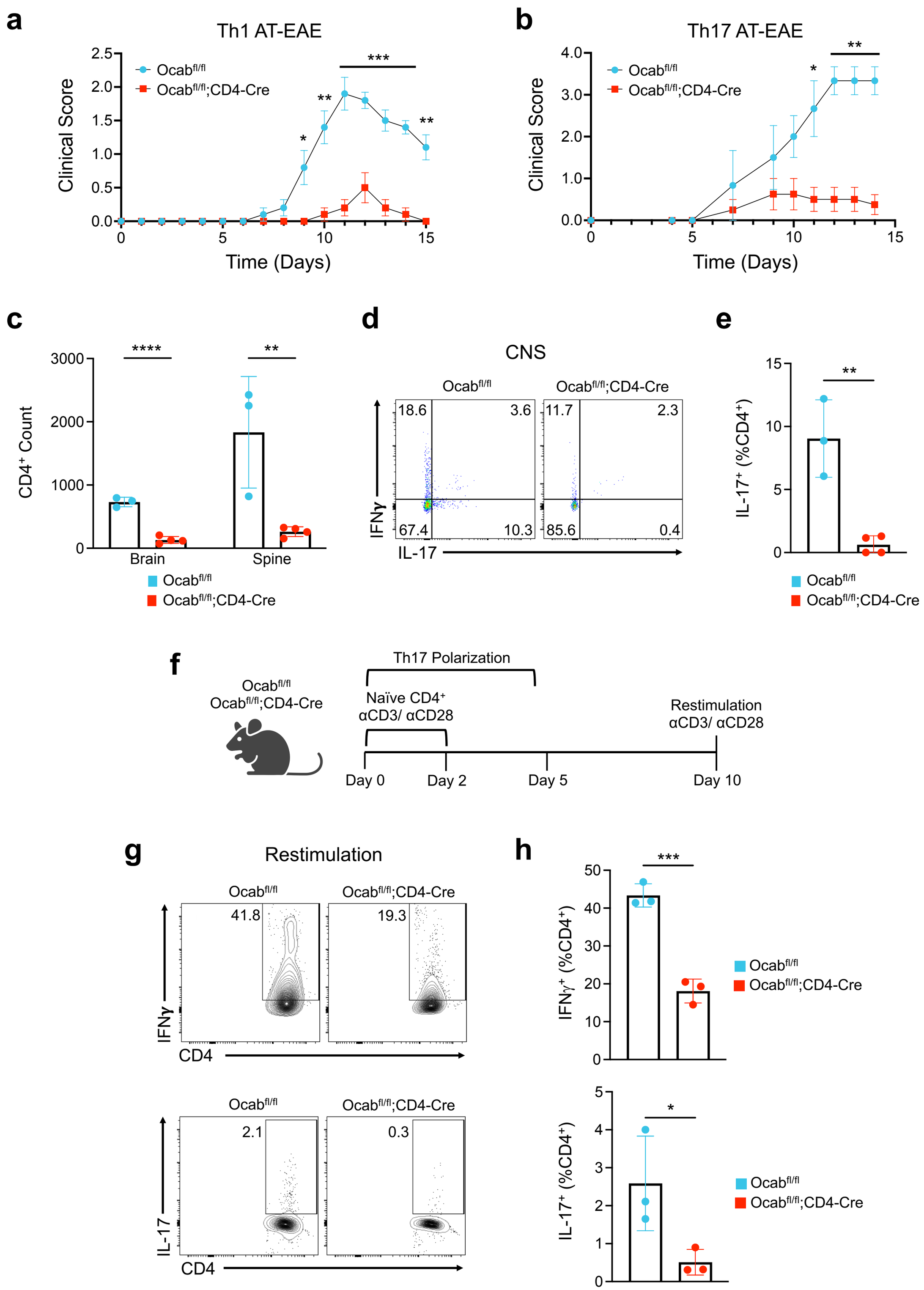
a
Th1 AT-EAE
Clinical Score
Time (Days)
Ocab$^{fl/fl}$
Ocab$^{fl/fl}$;CD4-Cre
b
Th17 AT-EAE
Clinical Score
Time (Days)
c
CD4$^+$ Count
Brain
Spine
d
CNS
IFNγ
IL-17
18.6
3.6
67.4
10.3
11.7
2.3
85.6
0.4
e
IL-17$^+$ (%CD4$^+$)
f
Ocab$^{fl/fl}$
Ocab$^{fl/fl}$;CD4-Cre
Th17 Polarization
Naïve CD4$^+$
αCD3/ αCD28
Restimulation
αCD3/ αCD28
Day 0
Day 2
Day 5
Day 10
g
Restimulation
41.8
19.3
2.1
0.3
CD4
h
IFNγ$^+$ (%CD4$^+$)
IL-17$^+$ (%CD4$^+$)

Fig. 3

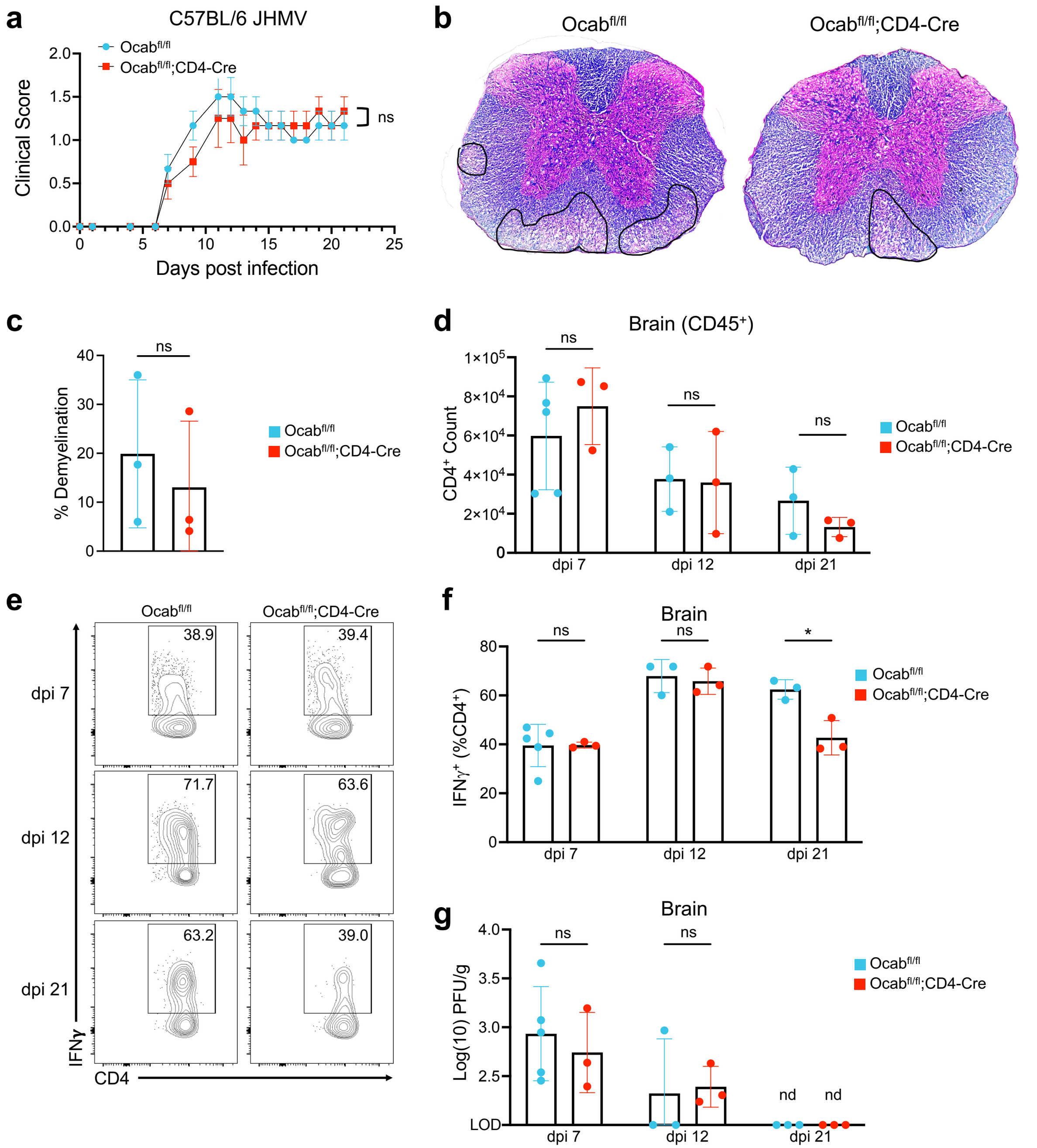
a
C57BL/6 JHMV
Ocab$^{fl/fl}$
Ocab$^{fl/fl}$;CD4-Cre
Clinical Score
2.0
1.5
1.0
0.5
0.0
0
5
10
15
20
25
Days post infection
ns
b
Ocab$^{fl/fl}$
Ocab$^{fl/fl}$;CD4-Cre
c
% Demyelination
40
30
20
10
0
ns
Ocab$^{fl/fl}$
Ocab$^{fl/fl}$;CD4-Cre
d
Brain (CD45$^+$)
CD4$^+$ Count
1×10^5
8×10^4
6×10^4
4×10^4
2×10^4
0
ns
ns
ns
dpi 7
dpi 12
dpi 21
Ocab$^{fl/fl}$
Ocab$^{fl/fl}$;CD4-Cre
e
Ocab$^{fl/fl}$
Ocab$^{fl/fl}$;CD4-Cre
dpi 7
dpi 12
dpi 21
38.9
39.4
71.7
63.6
63.2
39.0
IFNγ
CD4
f
Brain
IFNγ$^+$ (%CD4$^+$)
80
60
40
20
0
ns
ns
*
dpi 7
dpi 12
dpi 21
Ocab$^{fl/fl}$
Ocab$^{fl/fl}$;CD4-Cre
g
Brain
Log(10) PFU/g
4.0
3.5
3.0
2.5
LOD
ns
ns
nd
nd
dpi 7
dpi 12
dpi 21
Ocab$^{fl/fl}$
Ocab$^{fl/fl}$;CD4-Cre

Fig. 4

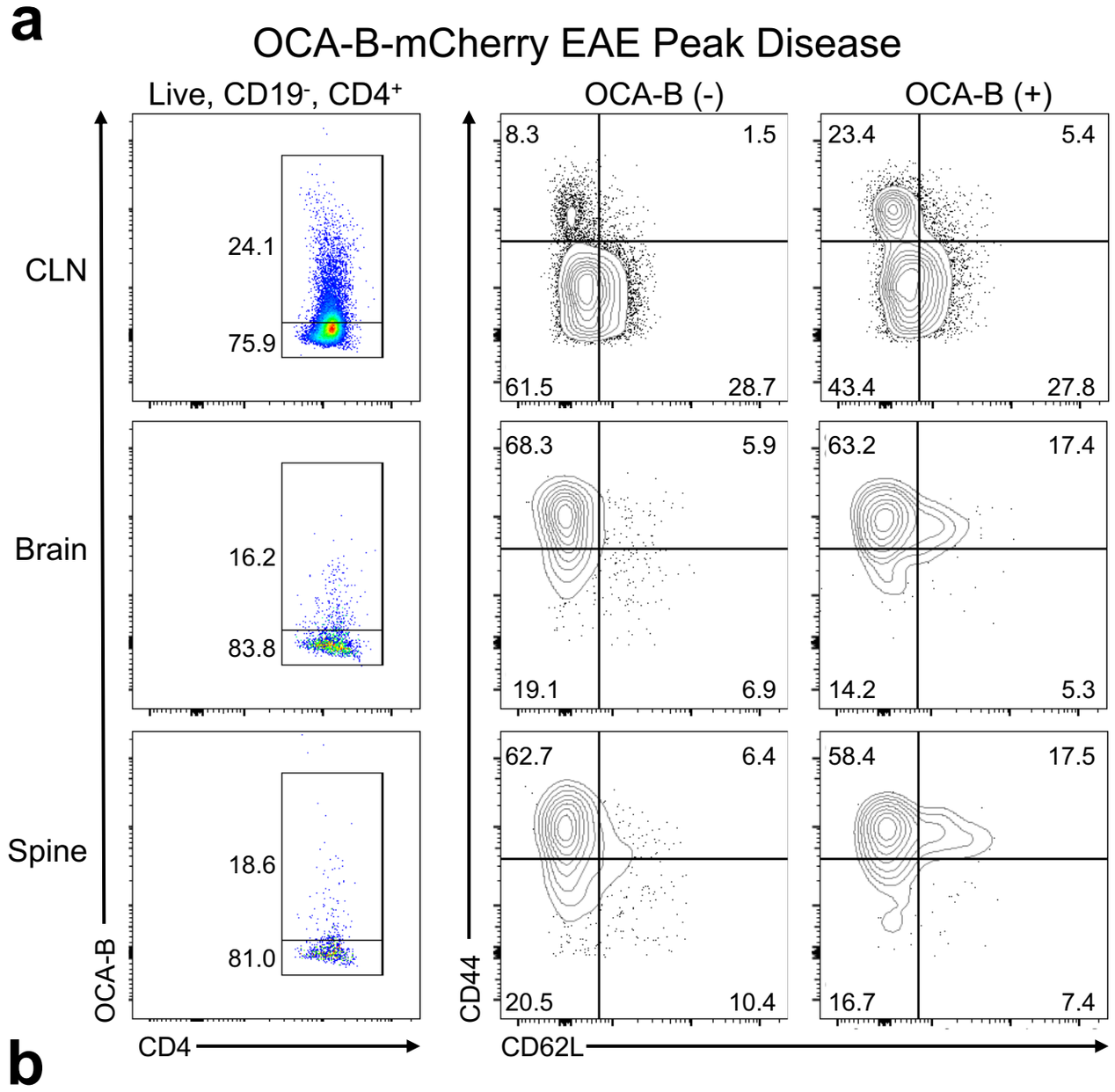

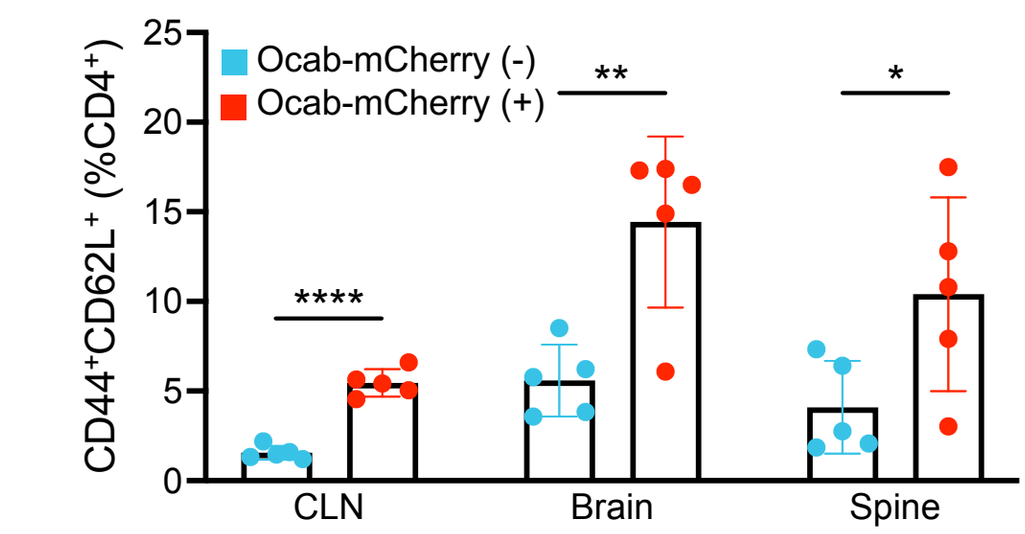

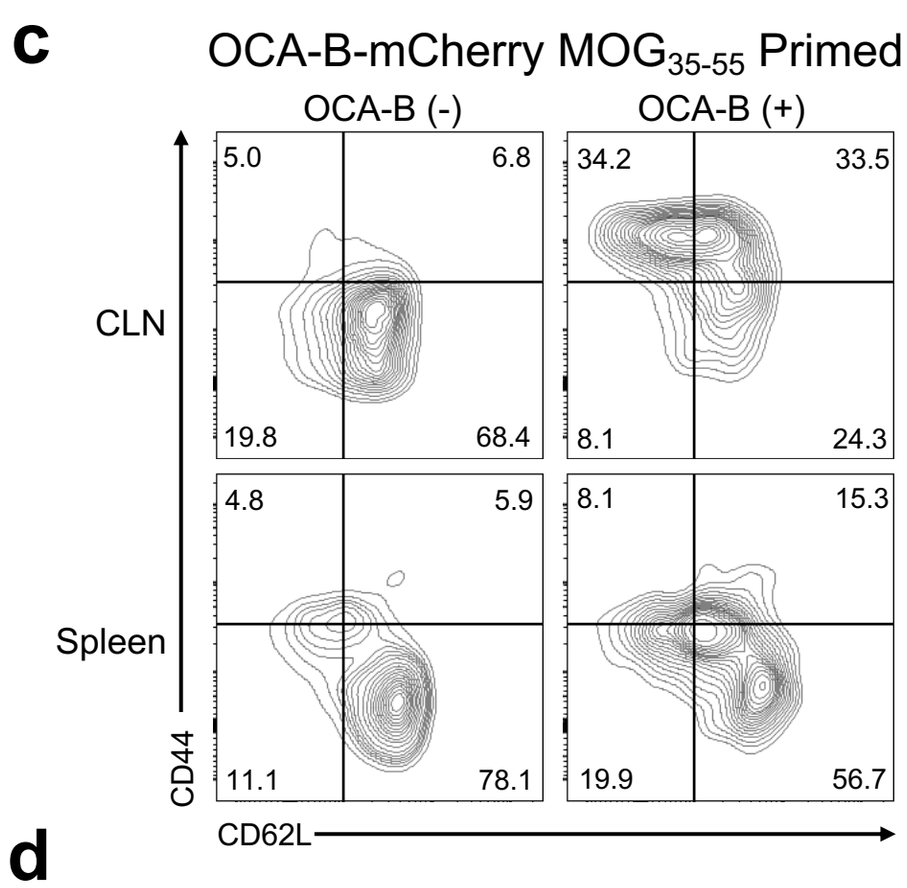

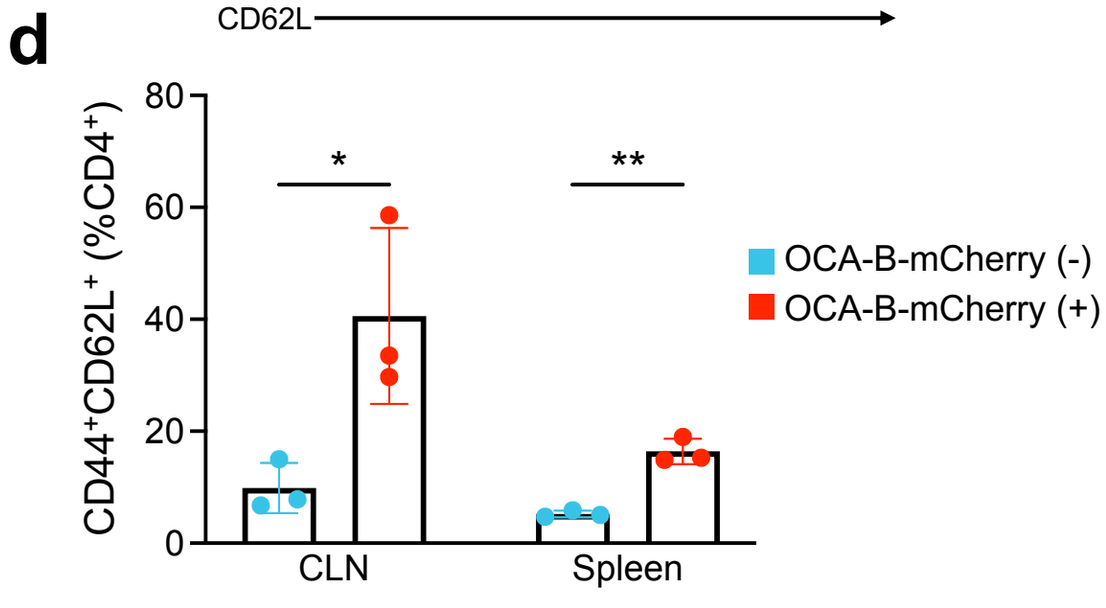

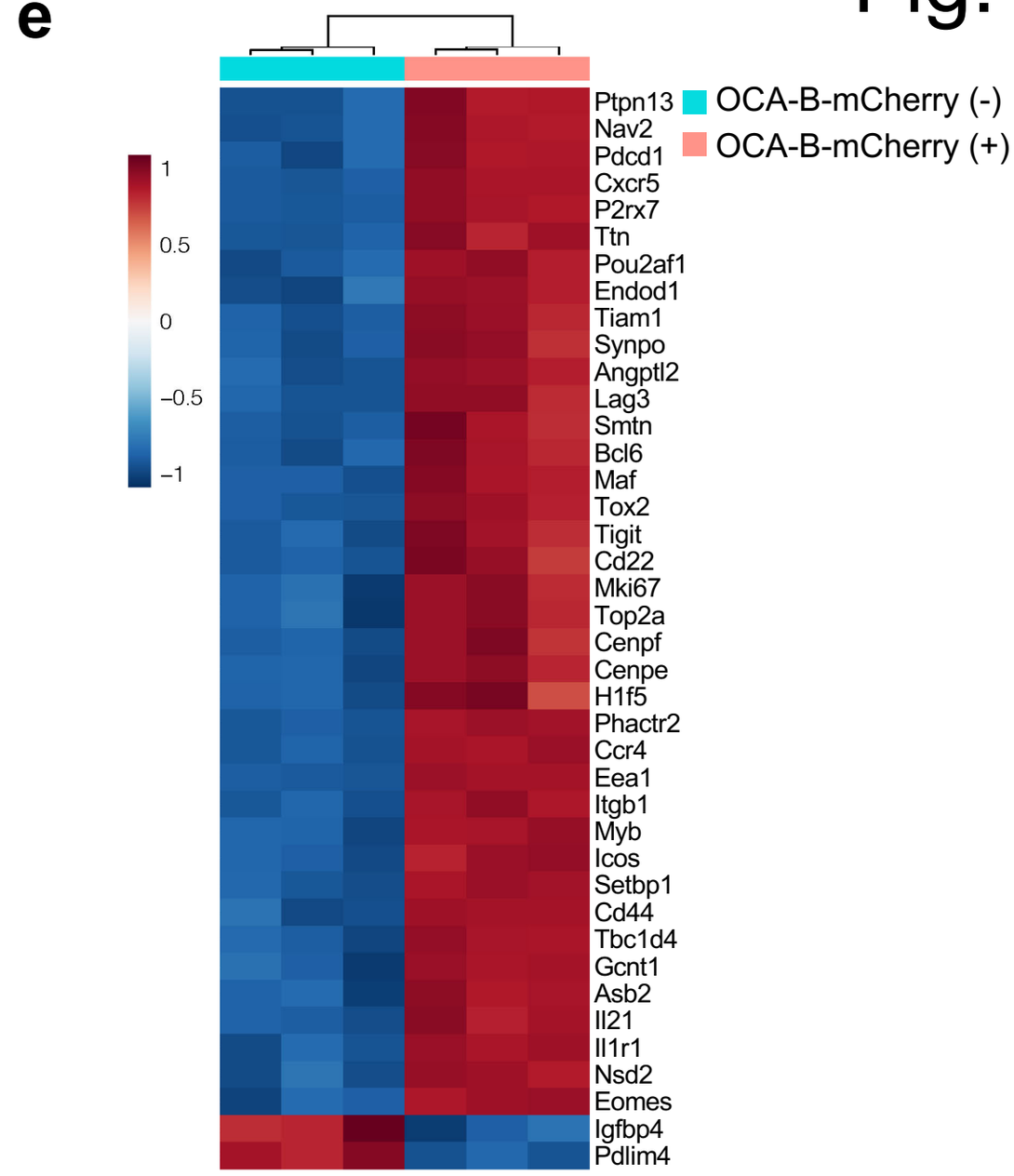

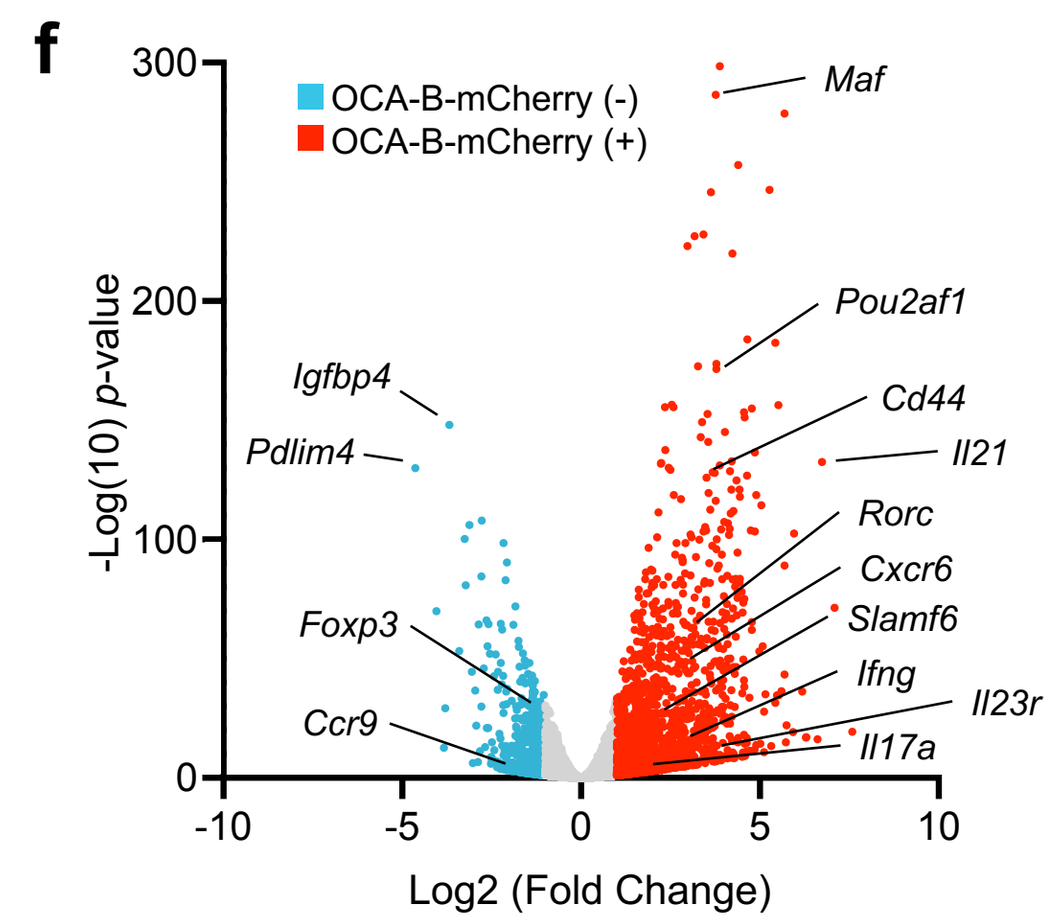

g

OCA-B⁺ Enriched Pathways

KEGG Pathway	*p*-value
Systemic Lupus Erythematosus	1.02E-04
Cytokine Cytokine Receptor Interaction	5.04E-04
Autoimmune Thyroid Disease	1.16E-03
Type I Diabetes Mellitus	2.06E-03
Cell Adhesion Molecules Cams	2.38E-03

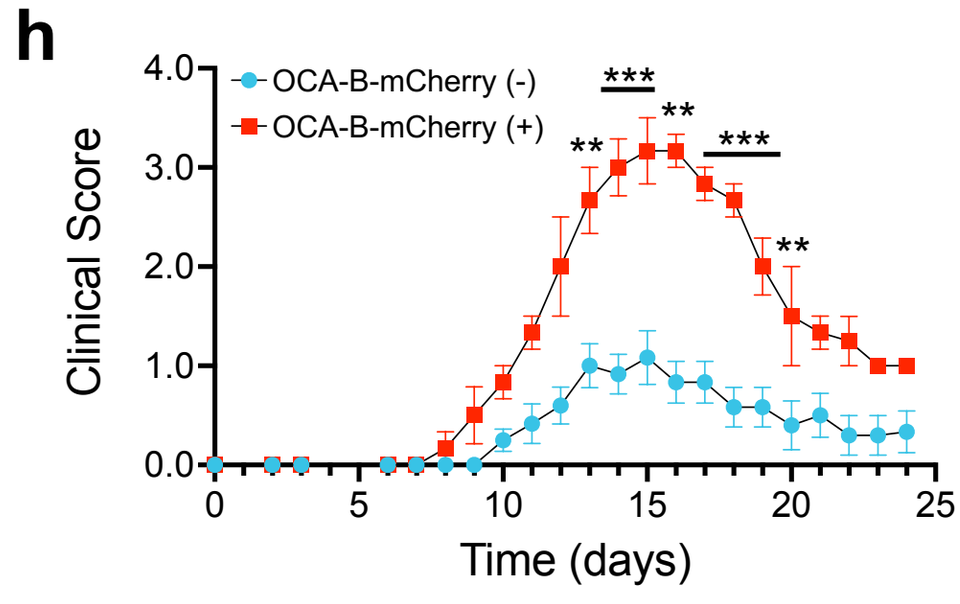

Fig. 5

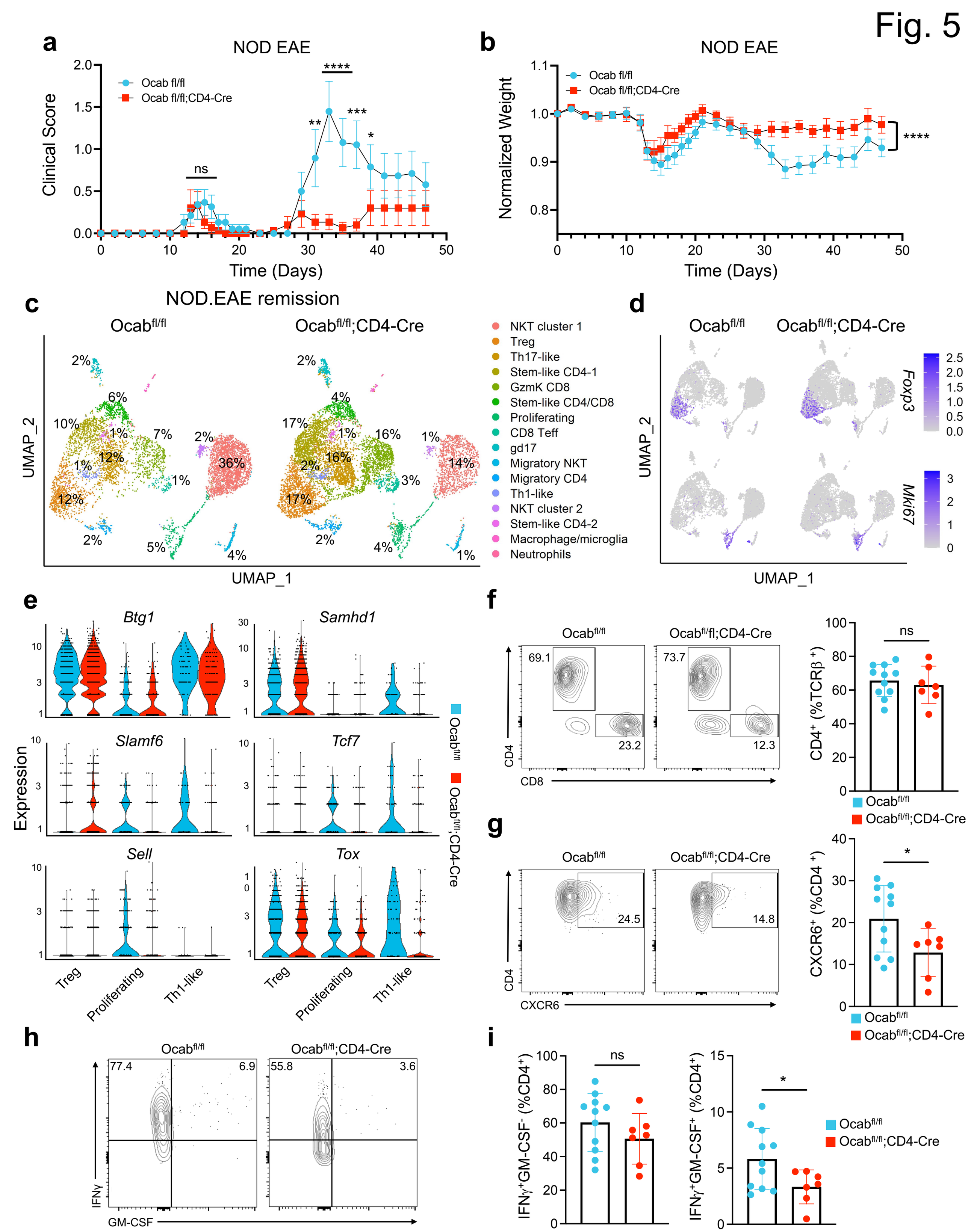
a
NOD EAE
Clinical Score
Time (Days)
Ocab fl/fl
Ocab fl/fl;CD4-Cre
ns
**
***
****
*
b
NOD EAE
Normalized Weight
Time (Days)
Ocab fl/fl
Ocab fl/fl;CD4-Cre
****
c
NOD.EAE remission
Ocabfl/fl
Ocabfl/fl;CD4-Cre
UMAP_1
UMAP_2
NKT cluster 1
Treg
Th17-like
Stem-like CD4-1
GzmK CD8
Stem-like CD4/CD8
Proliferating
CD8 Teff
gd17
Migratory NKT
Migratory CD4
Th1-like
NKT cluster 2
Stem-like CD4-2
Macrophage/microglia
Neutrophils
d
Ocabfl/fl
Ocabfl/fl;CD4-Cre
Foxp3
Mki67
UMAP_1
UMAP_2
e
Btg1
Samhd1
Slamf6
Tcf7
Sell
Tox
Expression
Treg
Proliferating
Th1-like
Ocabfl/fl
Ocabfl/fl;CD4-Cre
f
Ocabfl/fl
Ocabfl/fl;CD4-Cre
69.1
23.2
73.7
12.3
CD4
CD8
ns
CD4+ (%TCRβ+)
g
Ocabfl/fl
Ocabfl/fl;CD4-Cre
24.5
14.8
CD4
CXCR6
*
CXCR6+ (%CD4+)
h
Ocabfl/fl
Ocabfl/fl;CD4-Cre
77.4
6.9
55.8
3.6
IFNγ
GM-CSF
i
ns
IFNγ+GM-CSF- (%CD4+)
*
IFNγ+GM-CSF+ (%CD4+)
Ocabfl/fl
Ocabfl/fl;CD4-Cre

Fig. 6

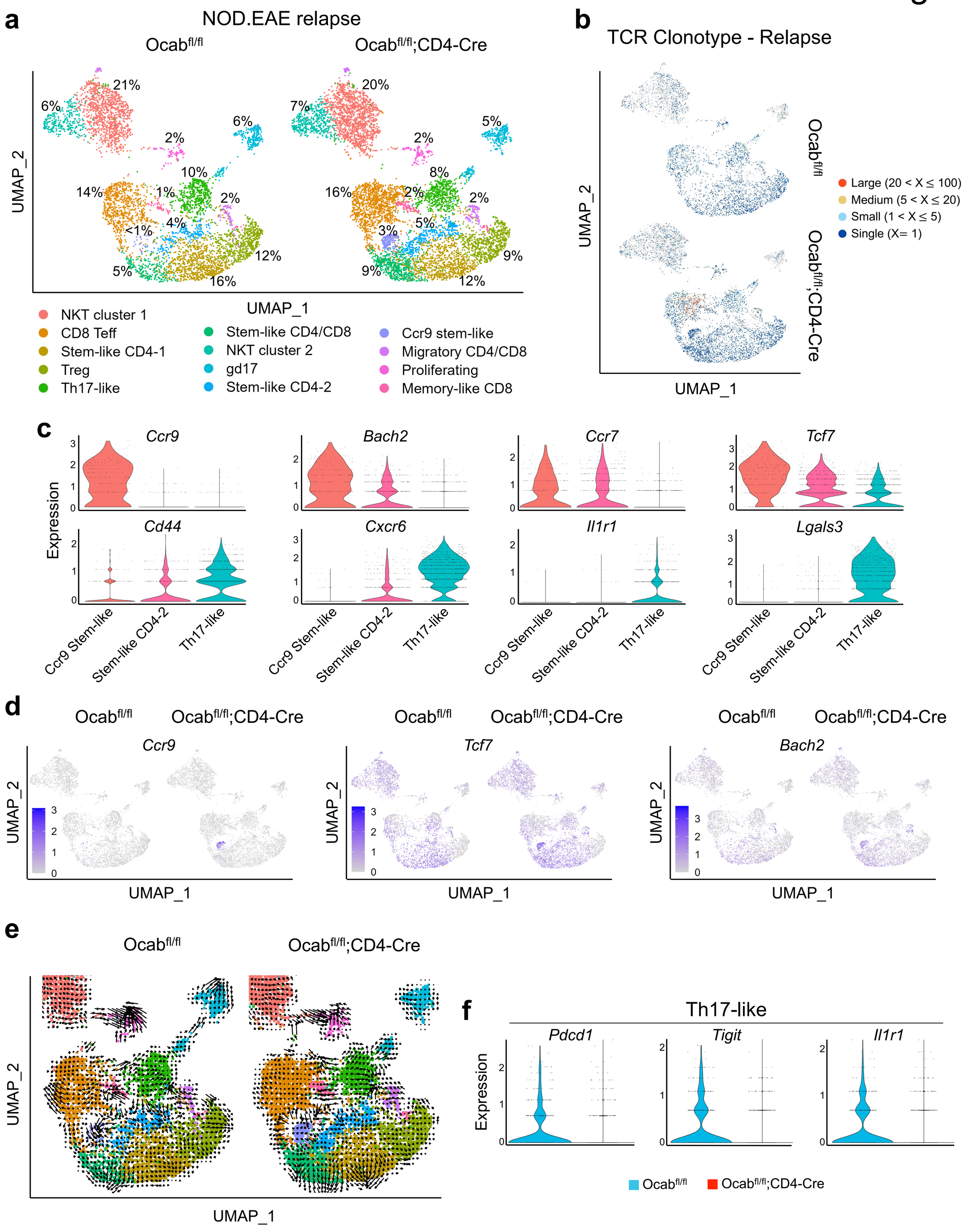
a
NOD.EAE relapse
Ocab fl/fl
Ocab fl/fl;CD4-Cre
UMAP_2
UMAP_1
21%
6%
2%
6%
10%
14%
1%
2%
4%
<1%
12%
5%
16%
20%
7%
2%
5%
8%
16%
2%
2%
5%
3%
9%
9%
12%
NKT cluster 1
CD8 Teff
Stem-like CD4-1
Treg
Th17-like
Stem-like CD4/CD8
NKT cluster 2
gd17
Stem-like CD4-2
Ccr9 stem-like
Migratory CD4/CD8
Proliferating
Memory-like CD8
b
TCR Clonotype - Relapse
Ocab fl/fl
Ocab fl/fl;CD4-Cre
Large (20 < X ≤ 100)
Medium (5 < X ≤ 20)
Small (1 < X ≤ 5)
Single (X= 1)
c
Ccr9
Bach2
Ccr7
Tcf7
Cd44
Cxcr6
Il1r1
Lgals3
Expression
Ccr9 Stem-like
Stem-like CD4-2
Th17-like
d
Ccr9
Tcf7
Bach2
e
f
Th17-like
Pdcd1
Tigit
Il1r1
Ocab fl/fl
Ocab fl/fl;CD4-Cre